Vapor-liquid interfacial properties of binary mixtures from molecular simulation and density gradient theory

Oliver Großmann, Simon Stephan*, Kai Langenbach[1], Hans Hasse

Laboratory of Engineering Thermodynamics (LTD), RPTU Kaiserslautern, Erwin-Schrödinger-Straße 44, 67663, Kaiserslautern, Germany

---

Abstract

Properties of the vapor-liquid interface of 16 binary mixtures were studied using molecular dynamics simulations and density gradient theory in combination with the PCP-SAFT equation of state. All binary combinations of the heavy-boiling components (cyclohexane, toluene, acetone, and carbon tetrachloride) with the light-boiling components (methane, carbon dioxide, hydrogen chloride, and nitrogen) were investigated at 0.7 times the critical temperature of the heavy-boiling component in the whole composition range. Data on the surface tension, the enrichment, the relative adsorption, and the interfacial thickness, as well as for the vapor-liquid equilibrium and Henry's law constant are reported. The binary interaction parameters were fitted to experimental data in a consistent way for all systems and both methods. Overall, the results from both methods agree well for all investigated properties. The interfacial properties of the different studied systems differ strongly. We show that these differences are directly related to the underlying phase equilibrium behavior.

Keywords: molecular simulation, density gradient theory, enrichment, adsorption, surface tension

---

*Corresponding author
Email address:* `simon.stephan@rptu.de` (Simon Stephan)
[1]Presently at the Chair for Thermal Process Engineering, University of Innsbruck, Innrain 52, 6020 Innsbruck, Austria

1. Introduction

Properties of vapor-liquid interfaces play an important role in many processes, such as mass transfer in distillation and absorption, wetting and adsorption, and bubble and droplet nucleation. Experimental studies of interfacial properties are generally limited to the surface tension, for which data on pure components are quite abundant, but data on mixtures are comparatively scarce.

Following the ideas of Gibbs, in phenomenological studies, the interface is generally treated as a two-dimensional object, whereas from an atomistic perspective, it is a three-dimensional region in which the properties change continuously from those in one bulk phase to those in the other. As the width of region is small, – it is typically of the order of a few nanometers – the gradients of the properties are very steep. Moreover, important fluctuations occur at fluid interfaces. Therefore, there are presently no experimental methods that can provide reliable information on the profiles of the properties in the interfacial region of molecular fluids.

However, detailed information on the interfacial region can be obtained from molecular simulations, density functional theory (DFT), and density gradient theory (DGT). The first requires a force field describing the interactions between the atomistic particles, the latter two require an equation of state (EOS) describing the free energy of the system. Many authors have studied the interfaces of fluid mixtures using these methods, cf. Ref. [1] for an overview.

Comprehensive studies of interfacial properties of mixtures of model fluids are available [2–15], in which the influence of various molecular parameters on the mixture's interfacial properties was elucidated. In most cases, mixtures of Lennard-Jones fluids were studied. In contrast, systematic studies on interfacial properties of mixtures of real substances are still scarce, which is why we have carried out such a study by modeling and simulation, to be able to provide both information on macroscopic and nanoscopic properties. Both molecular dynamics (MD) simulations and DGT were used. DGT was preferred over DFT, as it is

simpler and known to give good results for fluid systems. As the EOS, we have chosen PCP-SAFT, as it is a highly developed EOS based on molecular theory and good PCP-SAFT models for all pure components in our study were available in the literature.

Sixteen binary systems were studied: These are all possible binary combinations of the heavy-boiling components (cyclohexane, toluene, acetone, and carbon tetrachloride) with the light-boiling components (methane, carbon dioxide, hydrogen chloride, and nitrogen). The temperature T was always $T = 0.7 \times T_{c,1}$, where $T_{c,1}$ is the critical temperature of the heavy-boiling component (1), so that the light-boiling component (2) is always supercritical at the studied temperature.

Data on the surface tension, the enrichment, the relative adsorption, and the interfacial thickness were taken for all systems in a consistent manner, and complemented by data on the vapor-liquid equilibrium (VLE) and the Henry's law constant of the light-boiling component. The enrichment [1] is a measure for the presence and height of a local maximum in a component density profile in the interfacial region. At vapor-liquid interfaces, it is usually only observed for light-boiling components. There is a current discussion on the effects of the enrichment on the mass transfer through the interface [8, 9, 14, 16–21]. The enrichment of a component at the interface is related to its relative adsorption, but the two properties describe different aspects and are not redundant [1, 22–24]. The systems studied in the present work were chosen since in mixtures of supercritical components with liquid solvents, strong enrichment is expected, based on experience with model systems [1, 14, 25]. Furthermore, all components in the study are widely used, and they cover a wide range of molecular properties, such as the polarity. The results from this work provide new insights into interfacial properties of real mixtures in different ways: On the one side, the influence of a variation of the molecular properties can be studied (albeit not with mono-parametric variations as in the model systems) and the results can be compared to those from studies of model systems [14, 25], and, on the other side, information on the relation of the phase behavior of the studied systems with both macroscopic and

3

nanoscopic interfacial properties is gained.

2. Methods

2.1. Studied Binary Systems

All calculations were carried out at isothermal conditions at reduced temperatures of 0.7, i.e., $T = 0.7 \times T_{c,1}$, where $T_{c,1}$ is the critical temperature of the heavy-boiling component 1 (with exception of the Henry's law constants, which were studied as a function of temperature, cf. Section 2.5). The corresponding absolute temperatures are listed in Table 1. The temperature $T = 0.7 \times T_{c,1}$ is higher than the pure component critical point of all studied light-boiling components, i.e., the light-boiling component 2 is supercritical in all considered systems.

The temperature $0.7 \times T_{c,1}$ was chosen because it is used often in conceptual studies of "typical" vapor-liquid equilibria, i.e., Refs. [14, 26, 27], it is above the triple point for most substances, and, at the same time, far enough from the critical point for an accurate description by EOS.

The heavy-boiling components were chosen to cover a wide range of chemical behavior with respect to molar mass (light/heavy, e.g., acetone vs. CCl_4), polarity (apolar/polar, e.g., cyclohexane vs. acetone), and aromaticity (non-aromatic vs. aromatic, e.g., cyclohexane vs. toluene). Similar considerations hold for the selection of the light-boiling components, so that the 16 possible combinations of light-boiling and heavy-boiling components are representative of many industrially relevant mixtures, such as those occuring in absorption processes. Some of the mixtures studied in the present work have also been discussed in the literature in the context of natural gas purification by membranes (toluene+CO_2/CH_4) [28, 29], plasma etching in integrated circuit manufacturing (CCl_4+N_2) [30, 31], and cation exchange processes for the separation of metals (acetone+HCl) [32, 33].

4

Table 1: Critical temperatures (taken from the cited references) of the heavy-boiling components used in this work and the values of $0.7 \times T_{c,1}$, at which the interfacial properties of the respective mixtures were studied.

System	$T_{c,1}$ / K	$0.7 \times T_{c,1}$ / K	Ref.
cyclohexane + X	554	387.8	[34]
toluene + X	593	415.1	[35]
acetone + X	507.6	355.32	[36]
CCl_4 + X	556.4	389.48	[37]

2.2. Equation of State + Density Gradient Theory

2.2.1. PCP-SAFT

In this work, the PCP-SAFT equation of state was used, which refers to the Perturbed-Chain Statistical Associating Fluid Theory of Gross and Sadowski [38] with extensions for associating components [39] as well as quadrupole-quadrupole [40], dipole-dipole [41], and dipole-quadrupole [42] interactions. Within PCP-SAFT, the Helmholtz energy is modeled as

$$A = A^{id} + A^{hc} + A^{disp} + A^{assoc} + A^{DD} + A^{QQ} + A^{DQ}, \tag{1}$$

where the indices id, hc, disp, assoc, DD, QQ, and DQ denote contributions from the ideal gas, hard chain, dispersion, association, dipole-dipole interactions, quadrupole-quadrupole interactions, and dipole-quadrupole interactions, respectively.

For all pure components, at least three model parameters are required: the segment number m, segment diameter σ, and segment dispersion energy ε. For associating components, the effective association volume $\kappa^{A_i B_i}$ and association energy $\epsilon_i^{A_i B_i}$ are needed additionally, as well as the association scheme [43, 44]. For polar components, the dipole moment μ or quadrupole moment Q are additionally required. The pure component parameters used in this work were taken from the literature [38, 40, 41, 45–47] and are listed in Table 2.

The model used for CO_2 includes the quadrupolar term QQ, that for acetone the dipolar term DD. The

Table 2: PCP-SAFT and DGT pure component parameters used in this work.

Component	m	σ	ε	Ref.	κ	Ref.
-	-	Å	$k_B K$	-	$10^{-20} J\,m^5\,mol^{-2}$	-
Cyclohexane	2.5303	3.8499	278.11	[38]	34.07	[48]
Toluene	2.8149	3.7169	285.69	[38]	31.89	[49]
Acetone ^{c}	2.7447	3.2742	232.99	[41]	11.49	[50]
CCl_4	2.3252	3.8055	292.13	[47]	26.59	this work
CH_4	1	3.7039	150.03	[38]	1.973	[49]
CO_2 ^{a}	1.5131	3.1869	163.33	[40]	2.420	[51]
HCl ^{b}	1.5888	2.9567	206.91	[45]	2.013	[45]
N_2	1.2365	3.2975	89.492	[46]	1.167	this work

^{a} CO_2 was modeled with a quadrupole; $Q = 4.4\ D\text{Å}$.

^{b} HCl was modeled with one H-bond donor and one H-bond acceptor association site; $\kappa^{A_iB_i} = 5.7172 \times 10^{-4}$ and $\epsilon_i^{A_iB_i} = 1039.8\ k_B K$.

^{c} Acetone was modeled with a dipole; $\mu = 2.88\ D$.

model for HCl included an H-bond donor and an H-bond acceptor site.

Binary dispersive-repulsive interactions in the mixtures were modeled by the modified Lorentz-Berthelot [52, 53] combination rules

$$\sigma_{ij} = \frac{\sigma_{ii} + \sigma_{jj}}{2}\,, \tag{2}$$

$$\varepsilon_{ij} = \xi_{ij}\sqrt{\varepsilon_{ii}\varepsilon_{jj}}\,, \tag{3}$$

where ξ_{ij} is the binary interaction parameter in the mixture of components i and j. In this work, all ξ_{ij} parameter values were fitted to experimental data of the Henry's law constant (cf. Section 2.5). The ξ_{ij} parameter was treated as temperature-independent, i.e, a single constant value of ξ_{ij} was used for each binary system $i + j$. The values for ξ_{ij} obtained from the fit are listed in Table 5.

The PCP-SAFT equation of state was used for the calculation of phase equilibria (*pxy* phase diagrams and Henry's law constants) and it served as a starting point for the calculations in the interfacial region via density gradient theory.

2.2.2. Density Gradient Theory

Density gradient theory (DGT) is a framework that is widely used for modeling fluid interfaces. In DGT, the Helmholtz energy of the heterogeneous interface is described by a Taylor expansion around the homogeneous state, which is truncated after the second order term. For the calculation, the Helmholtz energy of the homogeneous bulk phase and the so-called influence parameter κ has to be known. In the case of a binary system with a planar interface, the equation describing the Helmholtz energy reduces to

$$a(\boldsymbol{\rho}) = a_0(\boldsymbol{\rho}) + \sum_{i=1}^{2} \sum_{j=1}^{2} \frac{1}{2} \, \kappa_{ij} \nabla \rho_i \cdot \nabla \rho_j. \tag{4}$$

Here, $a_0(\boldsymbol{\rho})$ is the Helmholtz energy density in the homogeneous bulk phase, ∇ is the gradient operator applied to the component densities ρ_i and ρ_j, and κ_{ij} is the component-specific influence parameter. For a more detailed discussion on the DGT framework, the reader is referred to Refs. [54–56].

The influence parameter was treated as density- and temperature-independent here. The cross-interaction influence parameters (κ_{ij} when $i \neq j$) were calculated from the pure component influence parameters (κ_{ii}, κ_{jj}) by the geometric mean combination rule (without introducing an additional binary interaction parameter) from

$$\kappa_{ij} = \sqrt{\kappa_{ii} \kappa_{jj}}. \tag{5}$$

The pure component influence parameters were in most cases taken from literature [45, 48–51], where they were fitted to experimental surface tension data of the pure components. The κ_{ij} values are reported together with the PCP-SAFT pure component parameters in Table 2. Only for the components N_2 and CCl_4, the influence parameter was fitted to literature surface tension data retrieved from the DIPPR database [57] in this work (cf. Supporting Information).

In this work, the DGT was used in combination with the PCP-SAFT equation of state (c.f. Section 2.2.1)

to calculate the (continuous) concentration profiles $\boldsymbol{\rho}(z)$ as a function of the spacial coordinate z in the interfacial region. The relationship between the spacial coordinate and density is given by [58]

$$\int_{z^0}^{z} \mathrm{d}z = \int_{\rho_{\mathrm{ref}}^0}^{\rho_{\mathrm{ref}}(z)} \sqrt{\Delta\Omega^{-1}(\boldsymbol{\rho}) \sum_{i=1}^{2}\sum_{j=1}^{2} \frac{\kappa_{ij}}{2} \frac{\mathrm{d}\rho_i}{\mathrm{d}\rho_{\mathrm{ref}}} \frac{\mathrm{d}\rho_j}{\mathrm{d}\rho_{\mathrm{ref}}}} \, \mathrm{d}\rho_{\mathrm{ref}} , \tag{6}$$

where $\boldsymbol{\rho}$ is the vector of component densities, ρ_i and ρ_j are the component densities of the components i and j, ρ_{ref} is the component density of a reference component, for which in the present work always the heavy-boiling component was chosen, and $\Delta\Omega(\boldsymbol{\rho})$ is the grand potential per volume, defined as

$$\Delta\Omega(\boldsymbol{\rho}) = a_0(\boldsymbol{\rho}) - \sum_{i=1}^{2} \rho_i \mu_i^{\mathrm{bulk}} + p^{\mathrm{s}} . \tag{7}$$

Here, $a_0(\boldsymbol{\rho})$ is the homogeneous Helmholtz energy at the local density vector, μ_i^{bulk} is the saturated bulk phase chemical potential of component i, and p^{s} is the saturation pressure. For the integration, an arbitrary starting point $\rho_{\mathrm{ref}}^0 = \rho_{\mathrm{ref}}(z^0)$ must be chosen.

From the density profiles, the surface tension, the relative adsorption, the enrichment, and the interfacial thickness were calculated as follows:

The surface tension γ at the binary VLE interface was calculated from [58]

$$\gamma = \int_{\rho_{\mathrm{ref}}''}^{\rho_{\mathrm{ref}}'} \sqrt{2\Delta\Omega(\boldsymbol{\rho}) \sum_{i=1}^{2}\sum_{j=1}^{2} \kappa_{ij} \frac{\mathrm{d}\rho_i}{\mathrm{d}\rho_{\mathrm{ref}}} \frac{\mathrm{d}\rho_j}{\mathrm{d}\rho_{\mathrm{ref}}}} \, \mathrm{d}\rho_{\mathrm{ref}} , \tag{8}$$

where the phase indices $'$ and $''$ refer to the bulk liquid and bulk vapor phase, respectively.

The relative Gibbs adsorption [59] at the interface was calculated from

$$\Gamma_i^{(j)} = -(\rho_i' - \rho_i'') \int_{-\infty}^{\infty} \left[\frac{\rho_j(z) - \rho_j'}{\rho_j' - \rho_j''} - \frac{\rho_i(z) - \rho_i'}{\rho_i' - \rho_i''} \right] \, \mathrm{d}z, \tag{9}$$

8

with the saturated component densities ρ_i' and ρ_i'' of the components $i = 1, 2$ in the bulk liquid and vapor

phases, respectively. In Eq. (9), $\Gamma_i^{(j)}$ is the relative adsorption of component i with respect to component

j. For the binary systems studied in this work, only the relative adsorption of the light-boiling component

$\Gamma_2^{(1)}$ was considered.

In a previous work of our group [22], the so-called enrichment E_i was introduced. The enrichment of a

component i is defined as the ratio of the highest local density of this component to the larger of its two

bulk phase component densities

$$E_i = \frac{\max(\rho_i(z))}{\max(\rho_i', \rho_i'')},\tag{10}$$

where the phase indices $'$ and $''$ denote the liquid and vapor phase, respectively.

The enrichment and the relative adsorption, while linked, contain distinctly different information [1,

22, 45]. The enrichment can by definition only assume values $E_i \geq 1$; for the limiting case of $E_i = 1$, no

enrichment is present, i.e., the component density profile in the interface does not exhibit a local maximum.

In binary systems, an enrichment exceeding 1 is only found for the light-boiling component (here: component

2); thus, only the quantity E_2 is relevant for this work. High values of E_2 up to 10 have been reported for

some mixtures in the literature, see Refs. [15, 21, 60–64].

The thickness of the planar interface was calculated using the 90-10% definition according to Lekner and

Henderson [65]. The effective interfacial thickness L_{10}^{90} is hereby taken as the distance between two points, at

which the total local density $\rho_{\text{tot}}(z) = \rho_1(z) + \rho_2(z)$ has changed 10% and 90% respectively of the difference

between the two bulk densities:

$$L_{10}^{90} = \left| z(\rho_{90}^{\text{tot}}) - z(\rho_{10}^{\text{tot}}) \right|,$$ (11)

$$\rho_{10}^{\text{tot}} = \rho_{\text{tot}}'' + 0.1(\rho_{\text{tot}}' - \rho_{\text{tot}}''),$$

$$\rho_{90}^{\text{tot}} = \rho_{\text{tot}}'' + 0.9(\rho_{\text{tot}}' - \rho_{\text{tot}}'').$$

The arbitrary z-axis zero point of the interfacial profiles from both MD and DGT was defined so that $z(\rho_{\text{tot}}^*) = 0$, where $\rho_{\text{tot}}^* = \rho_{\text{tot}}'' + 0.5(\rho_{\text{tot}}' - \rho_{\text{tot}}'')$.

2.3. Molecular Dynamics Simulations

Molecular dynamics (MD) simulations were used in this work for computing Henry's law constants, vapor-liquid equilibria, and interfacial properties. The MD simulations were carried out with the codes *ms2* [66, 67] (for determining the Henry's law constants) and *ls1 mardyn* [68] (for determining the interfacial properties and vapor-liquid equilibria).

All components were modeled as rigid multi-center Lennard-Jones (LJ) models with point charges, point dipoles, and point quadrupoles. An overview of the models is given in Table 3. They were taken from the MolMod database [69]. The force fields used in this work are united-atom force fields, i.e., hydrogen atoms are fused with the neighboring heavier atoms (except for HCl). For CH_4, the simple LJ potential [70] was used. For CO_2 the model of Merker et al. was used [71]. For nitrogen, a 2CLJQ model [70] was used. The cyclohexane model [72] consists solely of LJ interaction sites. The HCl and CCl_4 models [73, 74] consist of LJ sites and point charges (two and five, respectively). The toluene [73] and acetone [75] models consist of LJ sites as well as point dipoles (one each) and point quadrupoles (five and one, respectively). The force field models used in this work have been parameterized with respect to pure component VLE data (saturated liquid density and vapor pressure). They have been shown to yield excellent predictions for

different thermophysical properties (see, e.g., [46, 76–83]). The surface tension was not considered during the model development. For similar force fields, the surface tension is known to be about 20% above corresponding experimental data [22, 45, 82, 84–88]. In the following, the simulations techniques are briefly described; for more details, the reader is referred to Refs. [14, 89, 90].

Table 3: Pure component force field models used in this work (taken from the literature).

Comp.	Type	Ref.
Cyclohexane	6 LJ sites	[72]
Toluene	7 LJ sites with 1 dipole and 5 quadrupoles	[73]
Acetone	4 LJ sites with 1 dipole and 1 quadrupole	[75]
CCl_4	5 LJ sites with 5 point charges	[74]
CH_4	1 LJ site	[70]
CO_2	3 LJ sites with 1 quadrupole	[71]
HCl	1 LJ site with 2 point charges	[73]
N_2	2 LJ sites with 1 quadrupole	[70]

Henry's law constants H_{21} of the light-boiling component 2 in the solvent 1 were determined in the NpT ensemble with 864 solvent particles. In the simulations, the residual chemical potential μ_2^∞ of the solute was sampled using Widom's test particle method. Henry's law constants were then determined from

$$H_{2,1} = \rho' T \exp(\mu_2^\infty / T) \,, \tag{12}$$

where ρ' indicates the saturated liquid density of the solvent and T is the temperature. The equilibration of the pure component solvent was carried out for 60,000 time steps and the production was carried out for 500,000 time steps. The time step was 1.2 fs. The statistical uncertainty of the Henry's law constant was estimated to be three times the standard deviation of 50 block averages with the size of 10,000 time steps. The pressure of the NpT simulation was chosen to be 5% above the pure component vapor pressure of the solvent. The cut-off radius was 17.5 Å.

Analogously to the EOS, the binary dispersive-repulsive interactions in the MD simulations were modeled using the modified Lorentz-Berthelot [52, 53] combination rules (cf. Eq. (2)-(3)). Therein, a temperature-

11

independent fit parameter ξ_{ij} was used for each binary system $i + j$. In this work, all ξ_{ij} values were fitted to experimental data of the Henry's law constant (cf. Section 2.5). For each binary system, a single experimental data point was used. Iteratively, the binary interaction parameter ξ_{ij} was varied such that the Henry's law constant MD result was in good agreement with the experimental data point.

The simulations for the coexisting liquid and vapor phase were carried out in the NVT ensemble with 16,000 particles. The simulation scenarios were arranged with a liquid phase slab in the middle and a vapor phase on each side. Periodic boundary conditions were used in all directions. The equilibration was carried out for 10^6 time steps and the production was 2.5×10^6 time steps. The time step was 1.5 fs. A slab-based long-range correction [91, 92] was used.

The initial densities and compositions of the bulk phases were taken from the PCP-SAFT predictions. Both density and pressure profiles were sampled in 1,200 bins in z-direction (normal to the interface). In the production phase, the density and pressure profiles were sampled in block averages of 500,000 time steps. From each block averaged profile, various phase equilibrium properties were computed: the vapor pressure p^s, the saturated liquid and vapor density ρ' and ρ'', and the composition of the liquid and vapor phase $\boldsymbol{x}$ and $\boldsymbol{y}$. For this post-processing, the area close to the interface was excluded.

Moreover, from the pressure and density profiles, the vapor-liquid interfacial properties were computed, i.e., the surface tension, the relative adsorption, the enrichment, and the interfacial thickness. For the latter three, Eqs. (9)-(11) were used analogously to the DGT results evaluation.

The interfacial tension was obtained from the MD results by the mechanical route

$$\gamma = \frac{1}{2} \int_{-\infty}^{\infty} (p_\mathrm{N} - p_\mathrm{T}) \, \mathrm{d}z, \tag{13}$$

where p_N and p_T are the normal and transverse components of the pressure tensor [93].

The statistical uncertainties of the interfacial properties (γ, $\Gamma_2^{(1)}$, E_2, and L_{10}^{90}) as well as the bulk phase

properties (p^{s}, ρ', ρ'', $\boldsymbol{x}$, and $\boldsymbol{y}$) were estimated as three times the standard deviation of the sampled block average values.

2.4. Empirical Enrichment Model

In a previous work of our group [1], we have developed an empirical model for estimating the enrichment E_2 in binary systems. The model was trained to MD enrichment data of 90 different binary mixtures of Lennard-Jones fluids. In the present work, the predictions of this empirical enrichment model are compared to the predictions from PCP-SAFT + DGT and MD simulations for the 16 considered mixtures of real components.

As input, the model needs only information on bulk phase VLE properties, namely on the partition coefficient

$$K_2^{5\%} = \frac{y_2}{x_2 = 0.05 \ \mathrm{mol\,mol^{-1}}}, \tag{14}$$

evaluated at a liquid phase concentration of $x_2 = 0.05 \ \mathrm{mol\,mol^{-1}}$, and on (primarily the sign of) the component density difference of the light-boiling component between the liquid and vapor phase

$$\Delta\rho_2 = \frac{\rho_2' - \rho_2''}{\rho_{\mathrm{c},1}}. \tag{15}$$

The quantities $K_2^{5\%}$ and $\Delta\rho_2$ were obtained directly from the VLE computed by PCP-SAFT (cf. Section 2.2.1). From this, the model prediction $E_2 = f(x_2, K_2^{5\%}, \Delta\rho_2)$ was evaluated for all compositions and all mixtures studied. Hence, the empirical enrichment model was used as an alternative to DGT for estimating E_2.

13

2.5. Determination of the Binary Interaction Parameter ξ_{ij} from Data on Henry's Law Constants

The binary interaction parameters of PCP-SAFT as well as the binary interaction parameters of the force fields were fitted to experimental data on the Henry's law constant H_{21} of the light-boiling component 2 in the heavy-boiling solvent 1. Since the value of the Henry's law constant characterizes the interaction between solute particles solely with solvent particles, it is an excellent quantity for parameterizing the binary interaction parameter ξ_{ij} of models based on molecular thermodynamics.

The values of $H_{21}(T)$ were determined from solubility data from the literature, which are reported in various different ways. An overview of these definitions is given for example by Battino [94, 95]. Table 4 lists the available experimental data on gas solubility for all 16 studied binary systems. These data points were converted to Henry's law constants, which includes the extrapolation to infinite dilution, using the procedure detailed in the Supporting Information.

In Figure 1 of the results section, the H_{21} data are plotted together with the results from the adjusted force fields and PCP-SAFT models. Some obvious outliers, namely eleven experimental data points in the system toluene+CH_4 and three experimental data points in the system acetone+N_2, were excluded from the fitting procedure and are marked in the figure as such.

For the EOS, the optimal value of the binary interaction parameter ξ_{ij}^{EOS} was determined by a least-squares minimization of the relative errors between the predicted Henry's law constant and all available experimental $H_{21}(T)$ data (cf. Table 4) for each of the 16 binary systems.

For the force fields, the binary interaction parameter ξ_{ij}^{MD} was adjusted to a single data point of the Henry's law constant in each system. At the pertaining temperature, at least five MD simulations with different values of ξ_{ij} were carried out for H_{21}. The optimal value of ξ_{ij}^{MD} was then interpolated from these sampling points. For the assessment of that procedure and the quality of the obtained ξ_{ij}^{MD} value, the Henry's law constant was predicted in a wide temperature range using MD simulations (cf. Figure 1). The

Table 4: Experimental data on the solubility in all 16 studied binary mixtures. The data points are listed by the type of solubility coefficient reported in the original literature and include the number of data points as well as the temperature range covered. p-x is data from isothermal VLEs at low pressures; p/c data are ratios of the solute's partial pressure to its molarity in the liquid phase; loading is data reported as the mass ratio of solute to solvent in the liquid phase

Comp. 1	Comp. 2	T / K	Type	Ref.	# of Points
Cyclohexane	CH_4	291 - 310	Bunsen	[96]	3
		283 - 303	Ostwald	[97]	5
		303 - 423	p-x	[98, 99]	4
	CO_2	284 - 313	Ostwald	[100]	3
		283 - 392	Henry	[101, 102]	7
		283 - 311	p-x	[103–106]	11
		298	Bunsen	[107]	1
		293	p/c	[108]	1
	HCl	283 - 313	p-x	[109–112]	8
	N_2	298	Bunsen	[113]	1
		300 - 443	Henry	[114]	10
		298	Ostwald	[115, 116]	2
		283 - 308	p-x	[100, 103, 104, 117]	1
Toluene	CH_4	213 - 293	Bunsen	[118]	5
		284 - 333	Ostwald	[119, 120]	8
		278 - 423	p-x	[121–123]	8
	CO_2	198 - 298	Bunsen	[124, 125]	8
		275 - 328	Henry	[126–129]	10
		288 - 298	Ostwald	[130]	3
		293	p/c	[108]	1
		228 - 313	p-x	[106, 119, 131, 132]	8
	HCl	195 - 298	p-x	[109, 133–135]	15
	N_2	303 - 363	Henry	[136]	2
		293 - 298	Ostwald	[130]	2
		283 - 313	p-x	[119]	3
Acetone	CH_4	278 - 310	Bunsen	[96, 137]	8
		197 - 313	Ostwald	[138]	7
		263 - 293	p-x	[139]	3
	CO_2	293 - 298	Bunsen	[125, 140]	2
		293 - 395	Henry	[141–143]	10
		195 - 293	Kuenen	[144–146]	13
		273 - 298	Ostwald	[130, 147, 148]	4
		293	p/c	[108]	1
		293 - 303	p-x	[149]	2
	HCl	273 - 301	loading	[150]	2
	N_2	223 - 363	Henry	[116, 117, 136, 151]	10
		195 - 314	Ostwald	[130, 138, 152, 153]	15
CCl_4	CH_4	253 - 333	Ostwald	[138, 154]	8
		298	p-x	[96]	1
	CO_2	288 - 298	Ostwald	[130]	3
		298	Bunsen	[107]	1
		293	p/c	[108]	1
	HCl	293 - 298	Henry	[155]	4
		233 - 343	p-x	[109, 112, 133, 156, 157]	14
	N_2	253 - 333	Ostwald	[154, 158]	10
		298	p-x	[159]	1

results were compared with all available experimental data and the EOS results (see discussion below).

The fitted parameters ξ_{ij}^{EOS} and ξ_{ij}^{MD} are listed in Table 5 of the results section.

3. Results and Discussion

In the following, the results from the MD simulations and DGT in combination with the PCP-SAFT EOS are presented and compared for all studied systems. First, the results for the Henry's law constants are presented, then the p-x-y diagrams at $T = 0.7 \times T_{\text{c},1}$. After this, the results for the interfacial properties are presented. Furthermore, the numerical values of the results presented here are provided in a machine-readable format in the Supporting Information.

3.1. Henry's Law Constants

For an accurate representation of the mixture behavior, the binary interaction parameters ξ_{ij} were fitted to experimental data of the Henry's law constant H_{21} at different temperatures, cf. Section 2.5. The numeric values obtained from the parameter fitting are listed in Table 5 – for both the EOS and MD. As expected, the numerical values are not identical, as the binary interaction parameters from MD and EOS are not directly related to another, $\xi_{ij}^{\text{MD}} \neq \xi_{ij}^{\text{EOS}}$.

Figure 1 shows the results of the fit. Both the Henry's law constants from MD and the EOS are compared to experimental data from the literature. The results for all 16 binary systems are arranged in a 4x4 grid with systems with the same light-boiling component 2 arranged in rows and systems with the same heavy-boiling component 1 arranged in columns (the same layout will be used for the pxy phase diagrams and the interfacial properties). The temperatures studied in the simulations cover approximately the entire range from the triple point of the solvent to the critical point of the solvent. Furthermore, a gray dashed line marks the temperature $T = 0.7 \times T_{\text{c},1}$ (cf. Table 1), at which the interfacial properties were studied (results presented below).

16

Table 5: Binary interaction parameters for the equation of state (ξ_{ij}^{EOS}) and molecular simulations (ξ_{ij}^{MD}).

Comp. 1	Comp. 2	Fitted ξ_{ij}^{EOS}	Fitted ξ_{ij}^{MD}
Cyclohexane	CH_4	0.956	0.992
	CO_2	0.923	0.967
	HCl	0.882	1.1018
	N_2	0.842	1.0027
Toluene	CH_4	0.943	1.0133
	CO_2	0.983	0.924
	HCl	1.003	0.981
	N_2	0.854	0.985
Acetone	CH_4	0.995	1.0064
	CO_2	0.966	1.030
	HCl	1.258	1.355
	N_2	0.958	0.960
CCl_4	CH_4	0.964	1.0010
	CO_2	0.962	0.9861
	HCl	0.898	1.0952
	N_2	0.853	0.996

Overall, the results from both MD and EOS are in good agreement with the experimental data. In some cases, there are substantial deviations between experimental data sets published by different authors; such obvious outliers were not included in the parameter fit. The temperature dependency of the Henry's law constant is generally described well using a temperature-independent parameter ξ_{ij} in both model concepts. Experimental data are often only available in a narrow temperature range, but in all cases, the temperature dependence of the data is correctly represented. Both predictive methods – PCP-SAFT + DGT and MD simulations – agree well in their extrapolations outside of the experimentally investigated regions. Only in some systems (cyclohexane+CH_4, cyclohexane+CO_2, cyclohexane+HCl, toluene+CO_2, toluene+HCl) significant deviations between the MD and the EOS results are found – at high temperatures and far outside the region for which data were available and used for the parameter fit.

In the system acetone+HCl, experimental data are particularly scarce: Only two data points are available. A probable reason for the scarcity of experimental data in the acetone+HCl system is the possibility of the chemical condensation reaction of acetone to mesityl oxide and phorone in presence of acid catalysts [160].
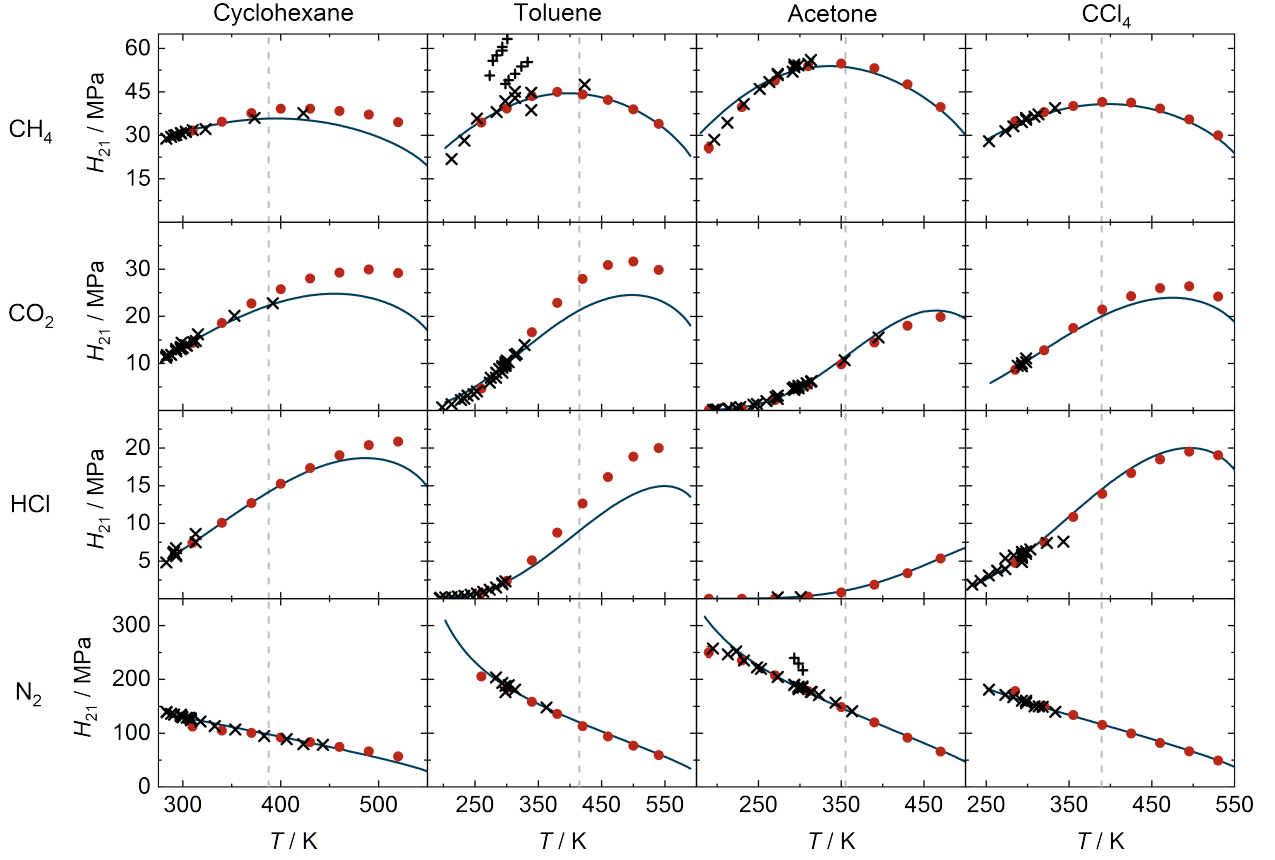
Figure 1: Henry's law constant in 16 binary systems as a function of the temperature. Data from molecular simulations (red circles) and PCP-SAFT (blue lines). Experimental data from the literature are marked with **x** where they have been used for the fitting procedure and with **+** where they have been excluded. Gray dashed lines mark the temperature $T = 0.7 \times T_{c,1}$.

Hence, it is unclear whether the experimental data are really for the solvent acetone or for mixtures of acetone and its reaction products – which were not considered in the model. Chemical reactions could also explain the unusually high corrections that had to be applied to the Lorentz-Berthelot combining rule to represent the two data points (values of $\xi_{ij} > 1.25$, cf. Table 5). Regardless, the results from the system acetone+HCl serve as an example for the (interfacial) properties of a binary system with two strongly interacting components, i.e., with strong attractive cross-interactions.

There is a noticeable similarity in the trends of the H_{21} curves for systems with the same light-boiling component. For example, all X+CH$_4$ systems exhibit a fairly symmetrical, near-parabolic trend of $H_{21}(T)$ with a maximum that is near $0.7 \times T_{c,1}$. The systems of X+CO$_2$ and X+HCl have asymmetric $H_{21}(T)$ curves

with the maximum of H_{21} being at much higher temperatures. The X+N$_2$ systems show a monotonously decreasing $H_{21}(T)$ curve, which is nearly linear in the entire temperature range. Hence, the nature of the light-boiling component dominates the gas solubility, which is in line with the results reported in Ref. [161].

The slope of the $H_{21}(T)$ curve is directly related to the enthalpy of absorption Δh^{abs} (cf. Supporting Information). A positive slope of $H_{21}(T)$, and thus $\Delta h^{\mathrm{abs}} < 0$, corresponds to exothermal absorption, and vice versa. At $T = 0.7 \times T_{\mathrm{c},1}$, exothermal absorption is found for all studied X+CO$_2$ and X+HCl systems. The inverse behavior, endothermal absorption, is found for all studied X+N$_2$ systems. For the X+CH$_4$ systems, the slope of the $H_{21}(T)$ curve is nearly zero, indicating a small enthalpy of absorption at $T = 0.7 \times T_{\mathrm{c},1}$.

The data allow for testing a hypothesis of Hayduk [162], who stated there might exist a common point of intersection in solubility data of different gases, measured in the same solvent, at the critical temperature of the solvent. The present data support this hypothesis, see Supporting Information.

3.2. Vapor-Liquid Equilibria

We have, furthermore, used the adjusted models to predict the complete isothermal vapor-liquid equilibria at the temperature of $T = 0.7 \times T_{\mathrm{c},1}$ using PCP-SAFT and MD simulations. The results are shown as *pxy*-diagrams in Figure 2.

The predictions from PCP-SAFT and MD are in very good agreement in the region of low to moderate pressures, which is as expected, as both models were fitted to the same type of experimental data The largest deviations are observed for the systems toluene+CO$_2$ and toluene+HCl and are directly connected to a mismatch of the $H_{21}(T)$ curves predicted by both models for $T = 0.7 \times T_{\mathrm{c},1}$, cf. Figure 1.

As expected, some differences between both methods are obsesrved upon approaching the critical point, where the EOS generally predicts higher pressures than the MD simulation, as has been widely discussed in the literature, and is due to the critical scaling behavior of the EOS [163–165].
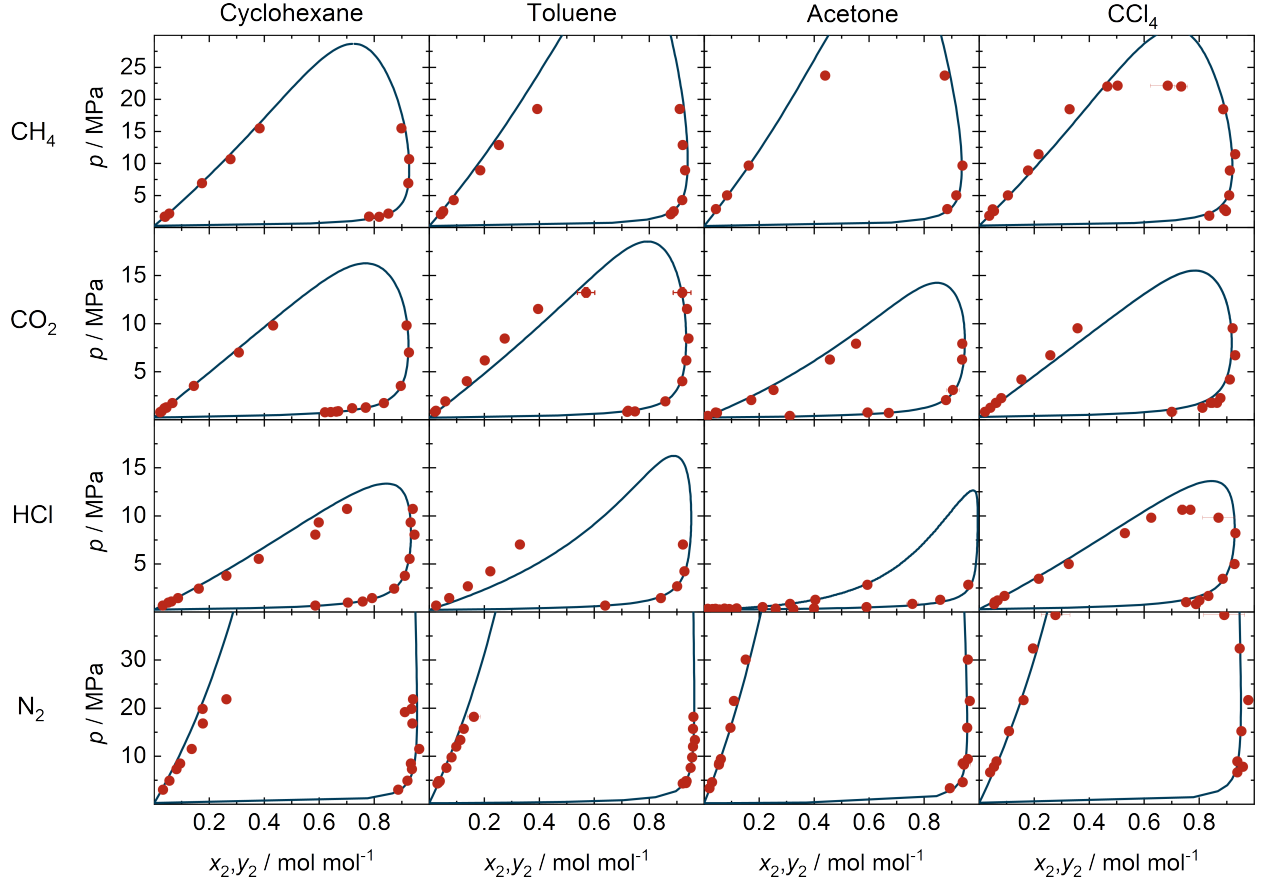
Figure 2: Vapor-liquid equilibria (plots of pressure vs. mole fraction of the light-boiling component) in 16 systems for $T = 0.7 \times T_{c,1}$. Blue lines are PCP-SAFT results and red circles are MD results.

Again, the results for the acetone+HCl system are particular: For one, the temperature $T = 0.7 \times T_{c,acetone} = 355.32$ K is only slightly higher than the critical temperature of HCl, which means that the phase envelope is only barely detached from the right edge of the diagram in Figure 2 and the binary critical point is very close to $x_2 = 1$ (PCP-SAFT predictions are $x_{HCl} = 0.98$ mol/mol at the binary critical point at $0.7 \times T_{c,1}$). On the other side of the diagram, at low x_2, the bubble and dew point curves are very close to another, which goes hand in hand with a small partition coefficient.

3.3. Interfacial Properties

3.3.1. Density Profiles

A representative plot of the density profiles at the interface obtained from the two methods is given in Figure 3 for the system toluene+CO_2 at $T = 0.7 \times T_{c,\text{toluene}}$. The component density profiles for toluene and CO_2, obtained from MD and the EOS, are plotted for the bulk liquid phase concentration $x_{CO_2} = 0.05$ mol/mol. The vapor phase is on the left and the liquid phase on the right side. For the density profile of the heavy-boiling component (toluene), a monotonous transition is observed, whereas the light-boiling (CO_2) component density profile exhibits a local maximum in the interfacial region, i.e., $E_2 > 1$.

For both components, the density profiles predicted by MD and DGT agree well. Both methods predict an enrichment peak in the CO_2 density profile but not in the toluene density profile. Furthermore, the predictions of both methods for the magnitude of this peak almost coincide. The width of the interfacial region is smaller for DGT than for MD, which is well known and related to the fact that fluctuations are present in the MD simulations but not in DGT, cf. Section 3.3.5 for more details. Good agreement of the interfacial density profiles predicted by MD and DGT has been observed in many previous studies [15, 22, 45, 166–169].
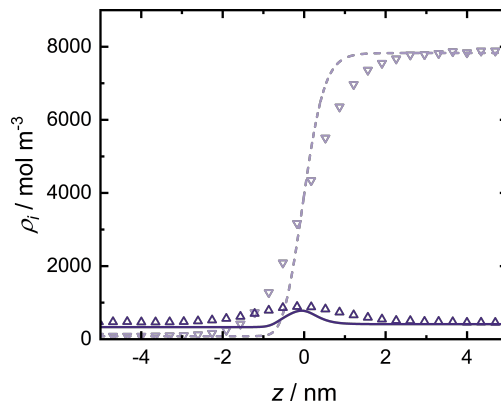

Figure 3: Vapor-liquid equilibrium density profile: Comparison of the DGT results (lines) to the MD results (symbols). $\triangle$ and solid line are CO_2, $\triangledown$ and dashed line are toluene. For better visibility, only every fifth MD data point is plotted. Results for $x_{CO_2} = 0.05$ mol/mol and $T = 0.7 \times T_{c,1}$.

In Figure 4, multiple density profiles over the entire investigated composition range are plotted for all 16 binary systems (only DGT results shown for clarity). The density of the heavy-boiling component is always much higher in the liquid phase than in the vapor phase. For the systems X+HCl, acetone+CO_2, and CCl_4+CO_2, this is also true for the light-boiling component ($\Delta\rho_2 \gg 0$), whereas the inverse trend ($\Delta\rho_2 < 0$) is observed for the systems X+N_2. For the systems X+CH_4, $\Delta\rho_2$ is only slightly positive, and for cyclohexane+CO_2 and toluene+CO_2, $\Delta\rho_2$ is nearly zero, switching sign from positive to negative with increasing liquid phase concentration x_2. There is a significant influence of the liquid phase concentration on both component density profiles. Moreover, in the systems X+N_2, a transition from VLE to LLE is observed, which has important consequences for the interfacial structure (cf. Figure 4). This has been analyzed recently by Nitzke et al. [170] for similar systems.
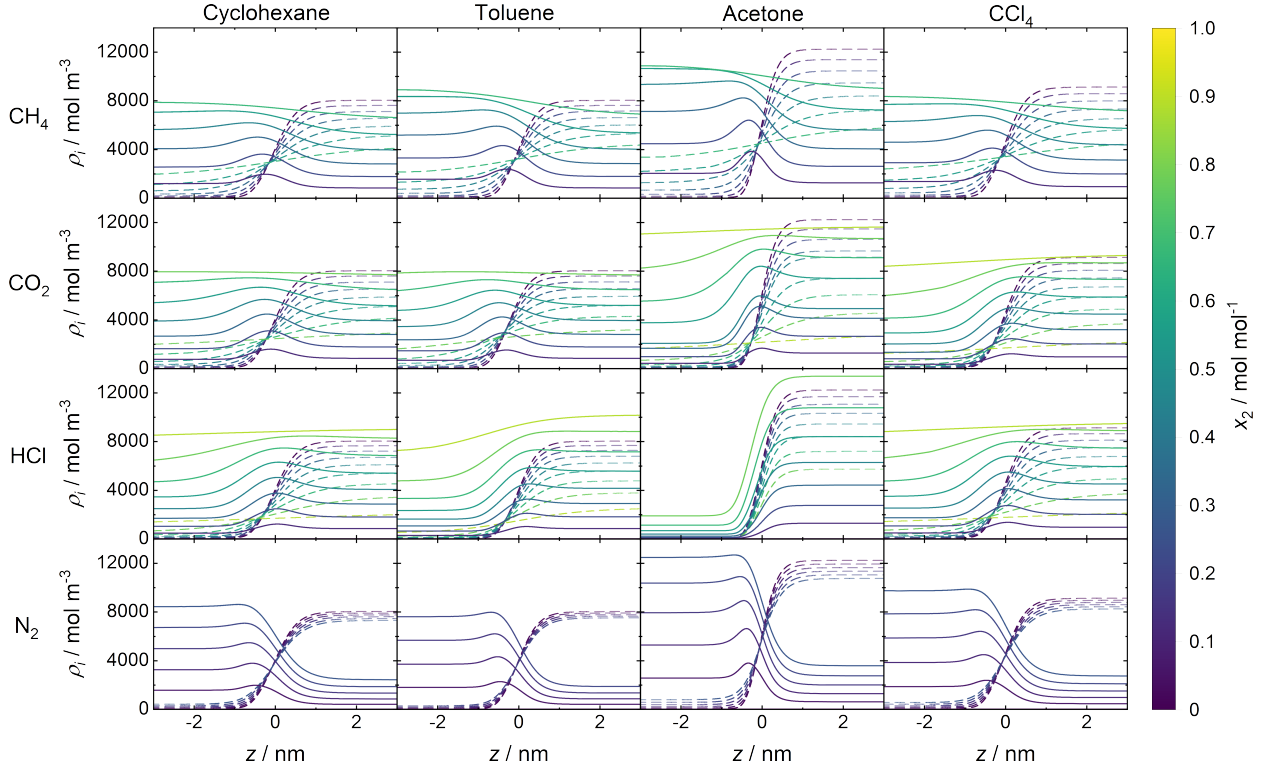

Figure 4: Component density profiles of the heavy-boiling component (dashed lines) and the light-boiling component (solid lines) in the 16 binary systems. Results from DGT at $T = 0.7 \times T_{c,1}$. The color indicates the liquid phase concentrations x_2.

3.3.2. Surface Tension

In Figure 5, the results of DGT and MD simulations for the surface tension γ are plotted. The highest values of the surface tension are found for the pure solvent (component 1). Upon adding the light-boiling component (component 2), the surface tension decreases monotonically until it becomes zero at the critical point of the mixture. The functions $\gamma(x_2)$ are nearly linear for most systems up to x_2 values that range from about 0.2-0.4 mol/mol, depending on the system (and on the choice of light-boiling component in particular). For higher values of x_2, the slope decreases until the critical point is reached.

The exception is again the system acetone+HCl: The surface tension results for that system exhibit a weak maximum. Such maxima are sometimes called positive aneotropic points and are usually associated with heavy-boiling azeotropes [15, 171–173]. Even though the system acetone+HCl does not have a heavy-boiling azeotrope at $T = 0.7 \times T_{c,1}$, it is close to having one (if the mixed interactions were only slightly more attractive). In line with this phase behavior, a positive aneotrope is predicted both by MD and DGT.

Figure 5 also includes experimental data for the surface tension of the pure solvents that were obtained from DIPPR correlations via the DIADEM data base [57]. Experimental mixture data on the surface tension of the studied systems are scarce and none are available at the temperatures investigated here. The values of the pure component surface tension are quite similar for all four solvents and range from 14.25 mN/m (cyclohexane) to 15.76 mN/m (acetone).

The DGT results match the experimental data perfectly, which is not astonishing as the influence parameter κ was fitted to these data, however, not necessarily at $T = 0.7 \times T_{c,1}$. The MD simulations systematically overestimate the surface tension throughout the entire composition range. The deviations for the mixture can be considered a consequence of the overestimation of the surface tension of the pure solvents. The overestimation is typically about 20%, which is in the range of what was also observed in the literature for MD simulations of many other systems [84, 174–176]. The reasons for this systematic overestimation are
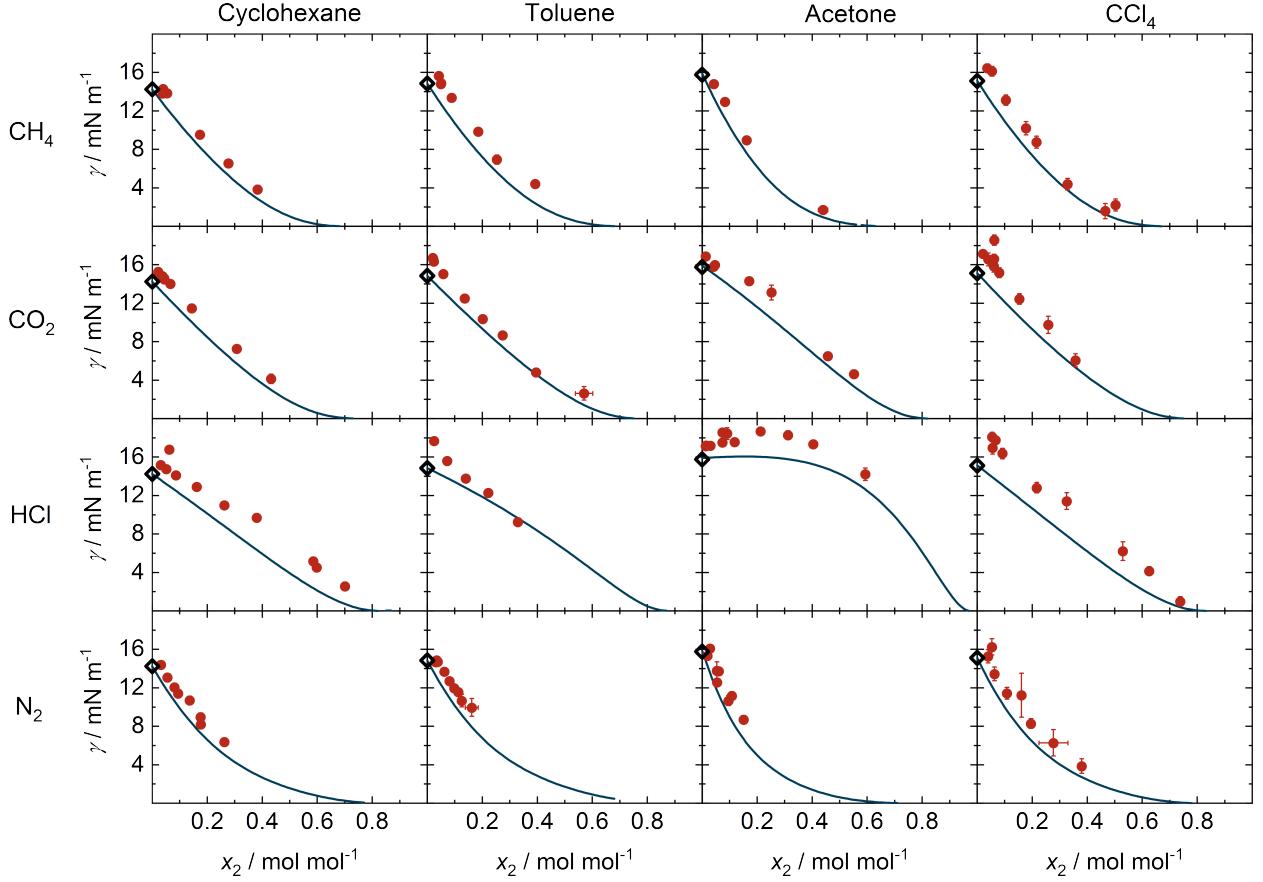
23

Figure 5: Surface tension γ in 16 binary systems plotted as a function of the liquid phase mole fraction of the light-boiling component x_2. The temperature is in all cases $T = 0.7 \times T_{c,1}$. Results from DGT (blue lines) and MD simulations (red circles). Experimental data from DIPPR correlations are shown as open black diamonds for the pure solvents.

still not well understood.

3.3.3. Relative Adsorption

The results for the relative adsorption of the light-boiling component with respect to the heavy-boiling component $\Gamma_2^{(1)}$ (cf. Eq. (9)) are shown as a function of the liquid phase mole fraction of the light boiling component x_2 in Figure 6. By definition, the relative adsorption is zero for the pure solvent and at the critical point. Between these, the relative adsorption $\Gamma_2^{(1)}$ is positive and has a maximum for all studied systems.

The MD and DGT results agree well, especially for the rising slope of the $\Gamma_2^{(1)}$ curves. On the falling
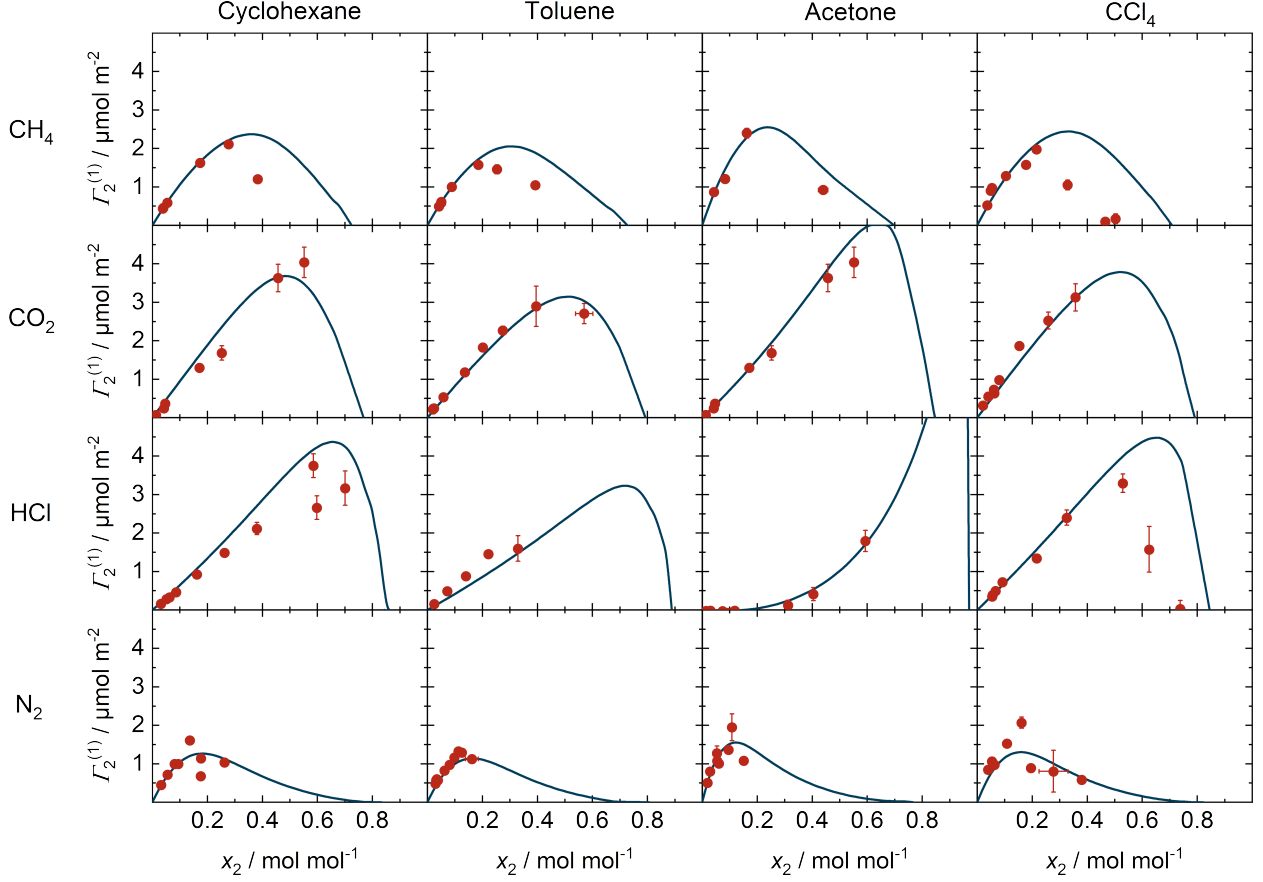
Figure 6: Relative adsorption $\Gamma_2^{(1)}$ in 16 binary systems plotted as a function of the liquid phase mole fraction of the light-boiling component x_2. Results from DGT (blue lines) and MD (red circles) for $T = 0.7 \times T_{c,1}$.

slope, MD simulations tend to predict the decline at lower values of x_2 than DGT. These differences may be related to the differences of the MD and EOS in describing the region near the critical point of the mixture, cf. Figure 2. However, in most studied cases, the phase equilibria obtained by MD and PCP-SAFT are in excellent agreement up to the concentration of the $\Gamma_2^{(1)}$ maximum $(x_2^{\max(\Gamma)})$. In these regions, the differences in absolute values of $\Gamma_2^{(1)}$ cannot be ascribed to the prediction of the bulk properties and must, hence, directly relate to the description of the interfacial properties.

The characteristics of the $\Gamma_2^{(1)}(x_2)$ curve seem to depend primarily on the light-boiling component. In systems X+CH$_4$ and X+N$_2$, we find moderately low values of $\Gamma_2^{(1),\max}$, as well as a moderately positive and strongly positive skew of the $\Gamma_2^{(1)}$-x_2 curves, respectively. In the systems X+CO$_2$ and X+HCl, we find

higher values of $\Gamma_2^{(1),\mathrm{max}}$ as well as negative skews of the $\Gamma_2^{(1)}$-x_2 curves. This again emphasizes the strong influence of the light-boiling component.

3.3.4. Enrichment

Figure 7 shows the results for the prediction of the enrichment E_2 of the light-boiling component by DGT and MD simulations. Additionally, the results of the empirical model for the prediction of E_2 [1] are shown. For all studied mixtures, the enrichment is largest for infinite dilution and decreases monotonously with increasing x_2 until it becomes zero at the critical point. This behaviour is as expected based on results for other systems [22, 45].
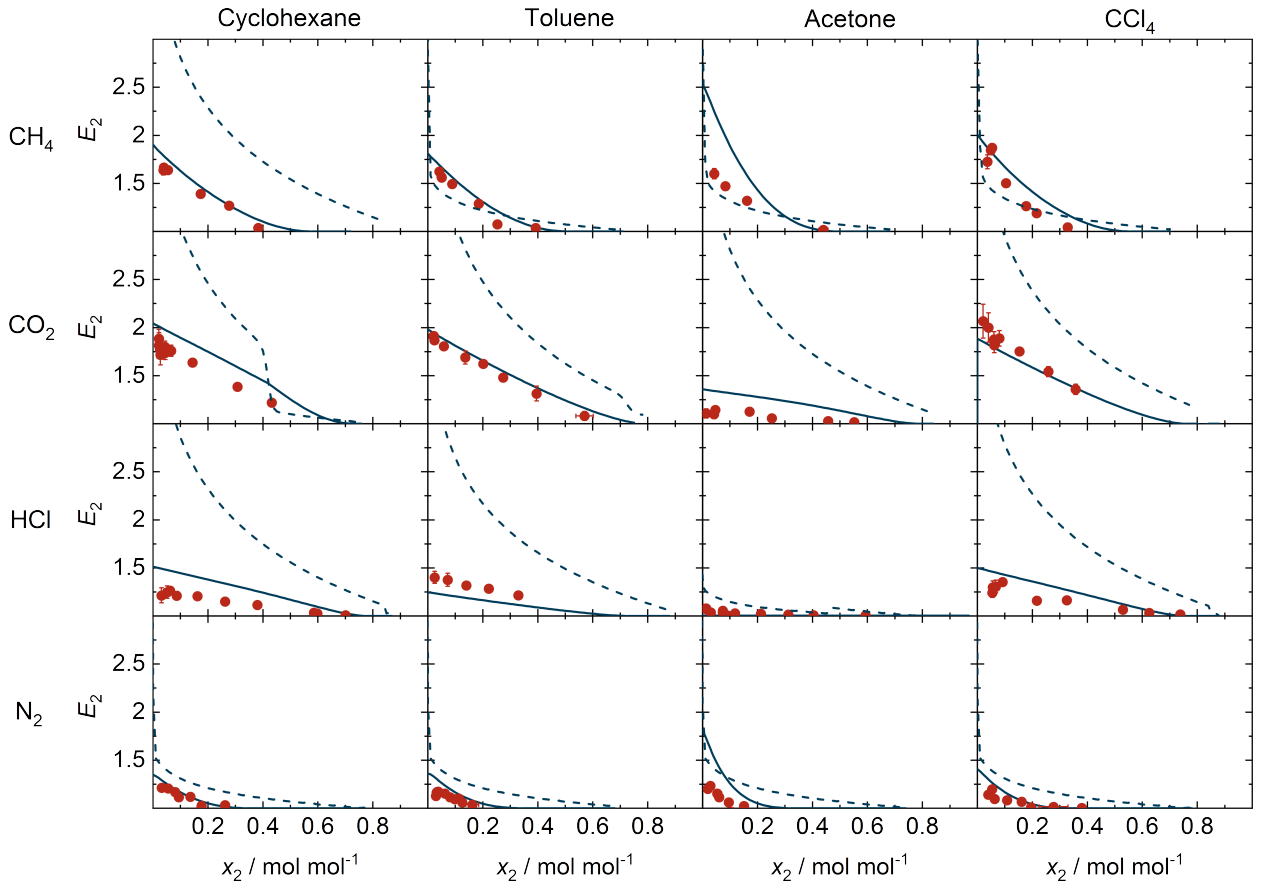
Figure 7: Enrichment E_2 in 16 binary systems plotted as a function of the liquid phase mole fraction of the light-boiling component x_2. Results from DGT (blue lines), MD simulations (red circles), and the empirical model (dashed lines) [1] at temperatures of $T = 0.7 \times T_{\mathrm{c},1}$.

For several of the studied systems, the MD and DGT results agree essentially within the MD uncertainties; in the other cases, DGT mostly predicts a slightly larger E_2 than MD. The empirical enrichment model systematically overestimates the enrichment in most cases.

Significant enrichment is found in the systems $X+CH_4$ and $X+CO_2$ (except acetone+CO_2), where the values of E_2 range between 1.5 and 2. Interestingly, very small enrichment is predicted for all $X+N_2$ systems – consistently from all three methods. The main difference between the $X+N_2$ systems and the other 12 systems is that, as a result of the low solubility, the vapor phase density of N_2 is significantly larger than the liquid phase ($\rho''_{N_2} > \rho'_{N_2}$) (cf. Figure 1). For model systems [25], it has been shown that when $\rho''_2 > \rho'_2$, i.e., $\Delta\rho < 0$, in binary systems of component 1 and 2 (2 being supercritical), low enrichment is obtained. This is confirmed in this work for real substance mixtures and also captured by the empirical enrichment model. On the other hand, the mixtures with significant enrichment have low absolute values of $\Delta\rho$ (the only exception being CCl_4+CO_2); in these cases, a relative adsorption must always lead to an enrichment [25, 177].

The system acetone+HCl is a special case among the 16 considered systems. Both MD and DGT likewise predict practically no enrichment (i.e., $E_2 = 1$) throughout the entire composition range. This is also predicted by the empirical enrichment model. It is important to note, that the same system does *not* exhibit a negligible relative adsorption – rather, it had the highest $\Gamma_2^{(1)}$ values of all studied systems (cf. Figure 6). The system acetone+HCl also behaves uniquely in respect to some other interfacial properties, such as the surface tension, which exhibits a local extremum (aneotrope).

3.3.5. Interfacial Thickness

Figure 8 shows the results of the interfacial thickness. Both MD and DGT results are shown.

For all pure solvents, the interfacial thickness is approximately 1 nm. In the mixtures, the interfacial thickness increases with increasing x_2 and exhibits a pole at the critical point. The agreement of the MD and
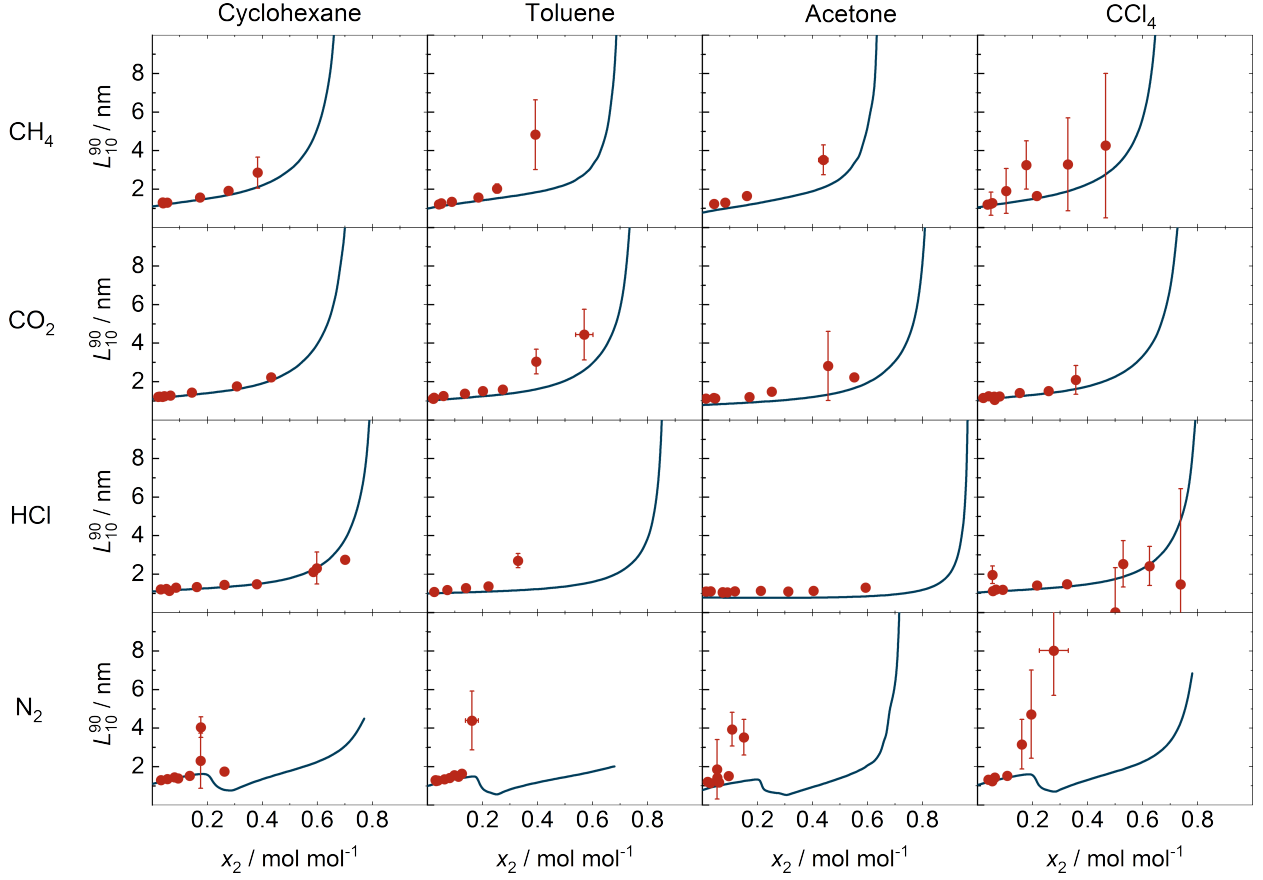
Figure 8: Interfacial thickness L_{10}^{90} as defined by [65] in 16 binary systems plotted as a function of the liquid phase mole fraction of the light-boiling component x_2. Results from DGT (blue lines) and MD simulations (red circles) for $T = 0.7 \times T_{c,1}$.

DGT results is generally good. Yet, the DGT results systematically underestimate the MD results, which is a consequence of the fact that the MD comprises fluctuations, whereas DGT does not [166, 178, 179]. As a result of these density fluctuations, which become increasingly relevant as the density difference between the two phases decreases (i.e., approaching the critical point), the error bars of the MD results near the critical point strongly increase. Significant deviations between the MD and the DGT results are observed at high concentrations in the systems toluene+CO_2 and acetone+HCl, which is where MD and PCP-SAFT are not in good agreement (cf. H_{21} data in Figure 1). The unexpected behavior of the DGT results for the X+N_2 systems is a direct consequence of the L_{10}^{90} definition and explained in the Supporting Information.

4. Conclusions

Vapor-liquid interfacial properties of binary systems were studied by MD and DGT. All 16 binary systems that can be obtained from combining the heavy-boiling components 1 (cyclohexane, toluene, acetone, and carbon tetrachloride) with the light-boiling components 2 (methane, carbon dioxide, hydrogen chloride, and nitrogen) were investigated. Results for the surface tension, relative adsorption, enrichment, and interfacial thickness are reported for $T = 0.7 \times T_{c,1}$. The pure component models were taken from the literature; for each binary system the interaction parameters of MD and DGT were adjusted to the same set of experimental gas solubility data. In general, good agreement between the predictions of the two independent methods was found.

The results for the interfacial properties can be compared in two ways: varying component 1 for given component 2, or vice versa. It is found that for a given light-boiling component 2, the variation of the heavy-boiling component 1 usually has only a minor influence – there may be some quantitative differences, but the qualitative features are the same. This is different, when for a given heavy-boiling component 1, the light-boiling component 2 is varied. Then, also the qualitative features of the studied interfacial properties often differ.

Among the studied systems, acetone+HCl plays a special role. Firstly, the experimental data base was very narrow for this system – and there is reason to believe that the experimental results might be affected by chemical reactions of acetone. While chemical reactions are not explicitly considered in the models of the present work, the high values of the binary interaction parameters for acetone+HCl obtained from the fit to the scarce data indicate unusually strong attraction. This has an important influence on all studied interfacial properties, which often differ qualitatively from those found for the other systems, in which the unlike interactions were less favorable.

The results for the surface tension are qualitatively similar for all systems: The surface tensions of the

pure components 1 are similar and adding component 2 leads to a decrease until the surface tension becomes zero at the critical point of the mixture. The variation of the results between the different studied systems is much stronger for the other studied interfacial properties. An exception is the system acetone+HCl, where a weak aneotrope was found, which is in line with the phase behavior in that system.

An enrichment of the light-boiling component 2 was found in all systems, except for acetone+HCl, with the highest numbers found for infinite dilution of component 2. The maximum enrichment is in the range of 1.5–2 for most studied systems; the values for the systems with nitrogen are lower throughout.

The magnitude of the relative adsorption and the enrichment of component 2 are not directly correlated, hence, these two quantities describe different aspects of the adsorption at the vapor-liquid interface.

The interfacial thickness is generally about 1–2 nm in all studied systems and increases beyond this only upon approaching the critical point of the mixture. The 10-90 definition for the interfacial thickness by Lekner and Henderson [65] leads to problems when the molar density of a component is similar in both phases.

Besides the data on the interfacial properties, also data on the Henry's law constants of the gas 2 in the solvent 1 H_{21} are provided, together with data on the vapor-liquid equilibria in the studied systems at $T = 0.7 \times T_{c,1}$. It would be interesting to study the influence of the temperature on the interfacial properties of the different systems in future work. Many of the studied systems show a maximum of $H_{21}(T)$. From the slope of $H_{21}(T)$ at $0.7 \times T_{c,1}$, the enthalpy of absorption can be calculated and is, depending on the system, either positive (endothermal absorption) or negative (exothermal absorption) or almost equal to zero. The enthalpy of absorption at $0.7 \times T_{c,1}$ was shown to primarily depend on the choice of the light-boiling component 2, which correlates to the features of the interfacial properties.

The results from the present study on interfacial properties of binary mixtures of real fluids with different types of interactions can be compared to results from previous studies on binary Lennard-Jones mixtures.

One could speculate that for systems with similar phase diagrams the interfacial properties are similar too. As a rule of thumb, this was found to be true, which indicates that mean field approximations are useful for a qualitative understanding of interfacial properties.

Acknowledgements

Data Availability Statement

The numerical data from Figures 1-8 are tabulated in a machine-readable form in the Supporting Information of this article. Furthermore, the numerical data of Figures S.1-S.6 of the Supporting Information are also tabulated there. Three .xlsx files are provided, depending on the method used to obtain the numerical data (EOS+DGT, MD simulations, other). Section S.6 of the Supporting Information discusses in detail the structure of the numerical data in the .xlsx files. Errorbars for the molecular simulation data in Figures 1-2 and Figures 5-8 indicate three standard deviations of the sampled block average values (cf. Section 2.3) and are also provided in the tabular Supporting Information.

References

[1] S. Stephan, H. Hasse, Enrichment at vapour–liquid interfaces of mixtures: Establishing a link between nanoscopic and macroscopic properties, International Reviews in Physical Chemistry 39 (3) (2020) 319–349. `doi:10.1080/0144235X.2020.1777705`.

[2] V. G. Baidakov, S. P. Protsenko, Molecular-dynamics investigation of phase equilibrium and surface tension in argon-neon system, The Journal of Physical Chemistry C 112 (44) (2008) 17231–17234. `doi:10.1021/jp805566g`.

[3] V. G. Baidakov, S. P. Protsenko, V. M. Bryukhanov, Relaxation processes at liquid-gas interfaces in one- and two-component Lennard-Jones systems: Molecular dynamics simulation, Fluid Phase Equilibria 481 (2019) 1–14. `doi:10.1016/j.fluid.2018.10.012`.

[4] S. P. Protsenko, V. G. Baidakov, Binary Lennard-Jones mixtures with highly asymmetric interactions of the components. 1. effect of the energy parameters on phase equilibria and properties of liquid-gas interfaces, Fluid Phase Equilibria 429 (2016) 242–253. `doi:10.1016/j.fluid.2016.09.009`.

[5] S. P. Protsenko, V. G. Baidakov, V. M. Bryukhanov, Binary Lennard-Jones mixtures with highly asymmetric interactions of the components. 2. effect of the particle size on phase equilibria and properties of liquid-gas interfaces, Fluid Phase Equilibria 430 (2016) 67–74. `doi:10.1016/j.fluid.2016.09.022`.

[6] F. J. Martinez-Ruiz, F. J. Blas, Interfacial properties of binary mixtures of square-well molecules from Monte Carlo simulation, The Journal of Chemical Physics 144 (15) (2016) 154705. `doi:10.1063/1.4947017`.

[7] M. M. Telo da Gama, R. Evans, Theory of the liquid-vapour interface of a binary mixture of Lennard-Jones fluids, Molecular Physics 41 (5) (1980) 1091–1112. `doi:10.1080/00268978000103811`.

[8] M. M. Telo da Gama, R. Evans, The structure and surface tension of the liquid-vapour interface near the upper critical end point of a binary mixture of Lennard-Jones fluids I. the two phase region, Molecular Physics 48 (2) (1983) 229–250. `doi:10.1080/00268978300100181`.

[9] D. J. Lee, M. M. Telo da Gama, K. E. Gubbins, The vapour-liquid interface for a Lennard-Jones model of argon-krypton mixtures, Molecular Physics 53 (5) (1984) 1113–1130. `doi:10.1080/00268978400102891`.

[10] D. J. Lee, M. M. Telo da Gama, K. E. Gubbins, Adsorption and surface tension reduction at the vapor-liquid interface, Journal of Physical Chemistry 89 (8) (1985) 1514–1519. `doi:10.1021/j100254a041`.

[11] S. Stephan, H. Hasse, Molecular interactions at vapor-liquid interfaces: Binary mixtures of simple fluids, Physical Review E 101 (2020) 012802. `doi:10.1103/PhysRevE.101.012802`.

[12] S. Stephan, H. Hasse, Influence of dispersive long-range interactions on properties of vapour-liquid equilibria and interfaces of binary Lennard-Jones mixtures, Molecular Physics 118 (9-10) (2020) e1699185. `doi:10.1080/00268976.2019.1699185`.

[13] S. Stephan, H. Hasse, Interfacial properties of binary mixtures of simple fluids and their relation to the phase diagram, Physical Chemistry Chemical Physics 22 (22) (2020) 12544–12564. `doi:10.1039/d0cp01411g`.

[14] S. Stephan, K. Langenbach, H. Hasse, Interfacial properties of binary Lennard-Jones mixtures by molecular simulation and density gradient theory, The Journal of Chemical Physics 150 (17) (2019) 174704. `doi:10.1063/1.5093603`.

[15] J. Staubach, S. Stephan, Interfacial properties of binary azeotropic mixtures of simple fluids: Moleculardynamics simulation and density gradient theory, Journal of Chemical Physics 157 (2022) 124702. `doi:10.1063/5.0100728`.

[16] D. Schaefer, S. Stephan, K. Langenbach, M. T. Horsch, H. Hasse, Mass transfer through vapor–liquid interfaces studied by non-stationary molecular dynamics simulations, The Journal of Physical Chemistry B 127 (11) (2023) 2521–2533. `doi:10.1021/acs.jpcb.2c08752`.

[17] C. Klink, J. Gross, A density functional theory for vapor-liquid interfaces of mixtures using the perturbed-chain polar statistical associating fluid theory equation of state, Industrial & Engineering Chemistry Research 53 (14) (2014) 6169. `doi:10.1021/ie4029895`.

[18] R. Nagl, P. Zimmermann, T. Zeiner, Interfacial mass transfer in water-toluene systems, Journal of Chemical & Engineering Data 65 (2) (2020) 328–336. `doi:10.1021/acs.jced.9b00672`.

[19] R. Nagl, T. Zeiner, P. Zimmermann, Interfacial mass transfer in quaternary liquid-liquid systems, Chemical Engineering and Processing - Process Intensification 171 (2022) 108501. `doi:https://doi.org/10.1016/j.cep.2021.108501`.

[20] J. M. Garrido, M. M. Piñeiro, A. Mejía, F. J. Blas, Understanding the interfacial behavior in isopycnic Lennard-Jones mixtures by computer simulations, Physical Chemistry Chemical Physics 18 (2016) 1114–1124. `doi:10.1039/C5CP06562C`.

[21] S. Enders, H. Kahl, Interfacial properties of water+alcohol mixtures, Fluid Phase Equilibria 263 (2) (2008) 160–167. `doi:10.1016/j.fluid.2007.10.006`.

[22] S. Becker, S. Werth, M. Horsch, K. Langenbach, H. Hasse, Interfacial tension and adsorption in the binary system ethanol and carbon dioxide: Experiments, molecular simulation and density gradient theory, Fluid Phase Equilibria 427 (2016)

476–487. `doi:10.1016/j.fluid.2016.08.007`.

[23] S. Stephan, H. Cardenas, A. Mejia, E. A. Mueller, The monotonicity behavior of density profiles at vapor-liquid interfaces of mixtures, Fluid Phase Equilibria 564 113596. `doi:10.1016/j.fluid.2022.113596`.

[24] S. Stephan, J. Staubach, H. Hasse, Review and comparison of equations of state for the Lennard-Jones fluid, Fluid Phase Equilibria 523 (2020) 112772. `doi:10.1016/j.fluid.2020.112772`.

[25] S. Stephan, H. Hasse, Molecular interactions at vapor-liquid interfaces: Binary mixtures of simple fluids, Physical Review E 101 (1) (2020) 012802. `doi:10.1103/PhysRevE.101.012802`.

[26] M. Heier, S. Stephan, F. Diewald, R. Müller, K. Langenbach, H. Hasse, Molecular dynamics study of wetting and adsorption of binary mixtures of the Lennard-Jones Truncated and Shifted fluid on a planar wall, Langmuir 37 (2021) 7405–7419. `doi:10.1021/acs.langmuir.1c00780`.

[27] J. Liu, M. Heier, W. G. Chapman, K. Langenbach, Adsorption in purely dispersive systems from molecular simulation, density gradient theory, and density functional theory, Journal of Chemical & Engineering Data 65 (3) (2020) 1222–1233. `doi:10.1021/acs.jced.9b00585`.

[28] Q. Liu, M. Galizia, K. L. Gleason, C. A. Scholes, D. R. Paul, B. D. Freeman, Influence of toluene on CO2 and CH4 gas transport properties in thermally rearranged (TR) polymers based on 3,3'-dihydroxy-4,4'-diamino-biphenyl (HAB) and 2,2'-bis-(3,4-dicarboxyphenyl) hexafluoropropane dianhydride (6FDA), Journal of Membrane Science 514 (2016) 282–293. `doi:10.1016/j.memsci.2016.04.043`.

[29] I. C. Omole, D. A. Bhandari, S. J. Miller, W. J. Koros, Toluene impurity effects on CO2 separation using a hollow fiber membrane for natural gas, Journal of Membrane Science 369 (1) (2011) 490–498. `doi:10.1016/j.memsci.2010.12.035`.

[30] T. P. Chow, P. A. Maciel, G. M. Fanelli, Reactive ion etching of silicon in CCl4 and HCl plasmas, Journal of The Electrochemical Society 134 (5) (1987) 1281. `doi:10.1149/1.2100658`.

[31] G. Smolinsky, R. A. Gottscho, S. M. Abys, Time-dependent etching of GaAs and InP with CCl4 or HCl plasmas: Electrode material and oxidant addition effects, Journal of Applied Physics 54 (6) (1983) 3518–3523. `doi:10.1063/1.332418`.

[32] J. S. Fritz, T. A. Rettig, Separation of metals by cation exchange in acetone-water-hydrochloric acid, Analytical Chemistry 34 (12) (1962) 1562–1566. `doi:10.1021/ac60192a016`.

[33] A. A. Larenkov, A. B. Bruskin, G. E. Kodina, Preparation of high-purity 68Ga solutions by ion exchange in mixed acetone-hydrochloric acid medium, Radiochemistry 56 (1) (2014) 57–65. `doi:10.1134/S1066362214010123`.

[34] D. R. Burgess, Thermochemical Data, in: P. J. Linstrom, W. G. Mallard (Eds.), NIST Chemistry WebBook, NIST Standard Reference Database Number 69, National Institute of Standards and Technology, Gaithersburg, MD.

[35] W. V. Steele, R. D. Chirico, S. E. Knipmeyer, N. K. Smith, NIPPR-395, Tech. rep. (1988).

[36] B. Galitzine, Über das Dalton'sche Gesetz, Annalen der Physik 277 (11) (1890) 588–626. `doi:10.1002/andp.18902771116`.

[37] V. Majer, V. Svoboda, Enthalpies of vaporization of organic compounds: A critical review and data compilation (Jan. 1986).

[38] J. Gross, G. Sadowski, Perturbed-chain SAFT: An equation of state based on a perturbation theory for chain molecules, Industrial & Engineering Chemistry Research 40 (4) (2001) 1244–1260. `doi:10.1021/ie0003887`.

[39] J. Gross, G. Sadowski, Application of the perturbed-chain SAFT equation of state to associating systems, Industrial & Engineering Chemistry Research 41 (22) (2002) 5510–5515. `doi:10.1021/ie010954d`.

[40] J. Gross, An equation-of-state contribution for polar components: Quadrupolar molecules, AIChE Journal 51 (9) (2005) 2556–2568. `doi:10.1002/aic.10502`.

[41] J. Gross, J. Vrabec, An equation-of-state contribution for polar components: Dipolar molecules, AIChE Journal 52 (3) (2006) 1194–1204. `doi:10.1002/aic.10683`.

[42] J. Vrabec, J. Gross, Vapor-liquid equilibria simulation and an equation of state contribution for dipole-quadrupole interactions, The Journal of Physical Chemistry B 112 (1) (2008) 51–60. `doi:10.1021/jp072619u`.

[43] W. G. Chapman, G. Jackson, K. E. Gubbins, Phase equilibria of associating fluids, Molecular Physics 65 (5) (1988) 1057–1079. doi:10.1080/00268978800101601.

[44] K. Langenbach, S. Enders, Cross-association of multi-component systems, Molecular Physics 110 (11-12) (2012) 1249–1260. doi:10.1080/00268976.2012.668963.

[45] S. Werth, M. Kohns, K. Langenbach, M. Heilig, M. Horsch, H. Hasse, Interfacial and bulk properties of vapor-liquid equilibria in the system toluene + hydrogen chloride + carbon dioxide by molecular simulation and density gradient theory + PC-SAFT, Fluid Phase Equilibria 427 (2016) 219–230. doi:10.1016/j.fluid.2016.07.016.

[46] J. Stoll, J. Vrabec, H. Hasse, Vapor–liquid equilibria of mixtures containing nitrogen, oxygen, carbon dioxide, and ethane, AIChE Journal 49 (8) (2003) 2187–2198. doi:10.1002/aic.690490826.

[47] I. A. Kouskoumvekaki, N. von Solms, M. L. Michelsen, G. M. Kontogeorgis, Application of the perturbed chain SAFT equation of state to complex polymer systems using simplified mixing rules, Fluid Phase Equilibria 215 (1) (2004) 71–78. doi:10.1016/S0378-3812(03)00363-7.

[48] O. G. Niño-Amézquita, S. Enders, P. T. Jaeger, R. Eggers, Interfacial properties of mixtures containing supercritical gases, The Journal of Supercritical Fluids 55 (2) (2010) 724–734. doi:10.1016/j.supflu.2010.09.040.

[49] O. G. Niño-Amézquita, S. Enders, P. T. Jaeger, R. Eggers, Measurement and prediction of interfacial tension of binary mixtures, Industrial & Engineering Chemistry Research 49 (2) (2010) 592–601. doi:10.1021/ie901209z.

[50] O. G. Niño-Amézquita, S. Enders, Prediction of interfacial tension of binary mixtures, Computer Aided Chemical Engineering 28 (2010) 85–90. doi:10.1016/S1570-7946(10)28015-X.

[51] J. Mairhofer, J. Gross, Modeling of interfacial properties of multicomponent systems using density gradient theory and PCP-SAFT, Fluid Phase Equilibria 439 (2017) 31–42. doi:10.1016/j.fluid.2017.02.009.

[52] H. A. Lorentz, Über die Anwendung des Satzes vom Virial in der kinetischen Theorie der Gase, Annalen der Physik 248 (1) (1881) 127–136. doi:10.1002/andp.18812480110.

[53] D. Berthelot, Sur le mélange des gaz, Comptes rendus hebdomadaires des séances de l'Académie des Sciences 126 (1898) 1703–1706.

[54] J. Rowlinson, B. Widom, Molecular Theory of Capillarity, Dover Publications, New York, 1982.

[55] P. M. W. Cornelisse, C. J. Peters, J. d. S. Arons, On the fundamentals of the gradient theory of van der Waals, The Journal of Chemical Physics 106 (23) (1997) 9820–9834. doi:10.1063/1.473872.

[56] C. Miqueu, B. Mendiboure, A. Graciaa, J. Lachaise, Modelling of the surface tension of pure components with the gradient theory of fluid interfaces: A simple and accurate expression for the influence parameters, Fluid Phase Equilibria 207 (1-2) (2003) 225–246. doi:10.1016/S0378-3812(03)00028-1.

[57] R. L. Rowley, W. V. Wilding, J. L. Oscarson, Y. Yang, N. A. Zundel, T. E. Daubert, R. P. Danner, DIPPR Data Compilation of Pure Chemical Properties, Design Institute for Physical Properties, AIChE (2003).

[58] C. Miqueu, B. Mendiboure, A. Graciaa, J. Lachaise, Modeling of the surface tension of multicomponent mixtures with the gradient theory of fluid interfaces, Industrial & Engineering Chemistry Research 44 (9) (2005) 3321–3329. doi:10.1021/ie049086l.

[59] J. W. Gibbs, The Scientific Papers of J. W. Gibbs, Dover Publications, 1961.

[60] T. Lafitte, B. Mendiboure, M. M. Piñeiro, D. Bessières, C. Miqueu, Interfacial properties of water/CO2: A Comprehensive description through a gradient theory–SAFT-VR Mie approach, The Journal of Physical Chemistry B 114 (34) (2010) 11110–11116. doi:10.1021/jp103292e.

[61] J. M. Míguez, J. M. Garrido, F. J. Blas, H. Segura, A. Mejía, M. M. Piñeiro, Comprehensive characterization of interfacial behavior for the mixture CO2 + H2O + CH4: Comparison between atomistic and coarse grained molecular simulation models and density gradient theory, The Journal of Physical Chemistry C 118 (42) (2014) 24504–24519. doi:10.1021/jp507107a.

[62] E. Schäfer, G. Sadowski, S. Enders, Interfacial tension of binary mixtures exhibiting azeotropic behavior: Measurement and modeling with PCP-SAFT combined with density gradient theory, Fluid Phase Equilibria 362 (2014) 151–162. doi:10.1016/j.fluid.2013.09.042.

[63] G. Niño-Amézquita, D. van Putten, S. Enders, Phase equilibrium and interfacial properties of water+CO2 mixtures, Fluid Phase Equilibria 332 (2012) 40–47. doi:10.1016/j.fluid.2012.06.018.

[64] O. G. Niño-Amézquita, S. Enders, Phase equilibrium and interfacial properties of water+methane mixtures, Fluid Phase Equilibria 407 (2016) 143–151. doi:10.1016/j.fluid.2015.05.005.

[65] J. Lekner, J. R. Henderson, Theoretical determination of the thickness of a liquid-vapour interface, Physica A: Statistical Mechanics and its Applications 94 (3) (1978) 545–558. doi:10.1016/0378-4371(78)90086-9.

[66] R. Fingerhut, G. Guevara-Carrion, I. Nitzke, D. Saric, J. Marx, K. Langenbach, S. Prokopev, D. Celný, M. Bernreuther, S. Stephan, M. Kohns, H. Hasse, J. Vrabec, ms2: A molecular simulation tool for thermodynamic properties, release 4.0, Computer Physics Communications 262 (2021) 107860. doi:10.1016/j.cpc.2021.107860.

[67] G. Rutkai, A. Köster, G. Guevara-Carrion, T. Janzen, M. Schappals, C. W. Glass, M. Bernreuther, A. Wafai, S. Stephan, M. Kohns, S. Reiser, S. Deublein, M. Horsch, H. Hasse, J. Vrabec, ms2: A molecular simulation tool for thermodynamic properties, release 3.0, Computer Physics Communications 221 (2017) 343–351. doi:10.1016/j.cpc.2017.07.025.

[68] C. Niethammer, S. Becker, M. Bernreuther, M. Buchholz, W. Eckhardt, A. Heinecke, S. Werth, H.-J. Bungartz, C. W. Glass, H. Hasse, J. Vrabec, M. Horsch, ls1 mardyn: The massively parallel molecular dynamics code for large systems, Journal of Chemical Theory and Computation 10 (10) (2014) 4455–4464. doi:10.1021/ct500169q.

[69] S. Stephan, M. T. Horsch, J. Vrabec, H. Hasse, MolMod – an open access database of force fields for molecular simulations of fluids, Molecular Simulation 45 (10) (2019) 806–814. doi:10.1080/08927022.2019.1601191.

[70] J. Vrabec, J. Stoll, H. Hasse, A set of molecular models for symmetric quadrupolar fluids, The Journal of Physical Chemistry B 105 (48) (2001) 12126–12133. doi:10.1021/jp012542o.

[71] T. Merker, C. Engin, J. Vrabec, H. Hasse, Molecular model for carbon dioxide optimized to vapor-liquid equilibria, The Journal of Chemical Physics 132 (23) (2010) 234512. doi:10.1063/1.3434530.

[72] T. Merker, J. Vrabec, H. Hasse, Molecular simulation study on the solubility of carbon dioxide in mixtures of cyclohexane+cyclohexanone, Fluid Phase Equilibria 315 (2012) 77–83. doi:10.1016/j.fluid.2011.11.003.

[73] Y.-L. Huang, M. Heilig, H. Hasse, J. Vrabec, Vapor–liquid equilibria of hydrogen chloride, phosgene, benzene, chlorobenzene, ortho-dichlorobenzene, and toluene by molecular simulation, AIChE Journal 57 (4) (2011) 1043–1060. doi:10.1002/aic.12329.

[74] G. Guevara-Carrion, T. Janzen, Y. M. Muñoz-Muñoz, J. Vrabec, Mutual diffusion of binary liquid mixtures containing methanol, ethanol, acetone, benzene, cyclohexane, toluene, and carbon tetrachloride, The Journal of Chemical Physics 144 (12) (2016) 124501. doi:10.1063/1.4943395.

[75] T. Windmann, M. Linnemann, J. Vrabec, Fluid phase behavior of nitrogen + acetone and oxygen + acetone by molecular simulation, experiment and the Peng–Robinson equation of state, Journal of Chemical & Engineering Data 59 (1) (2014) 28–38. doi:10.1021/je400691f.

[76] J. Vrabec, J. Stoll, H. Hasse, Molecular models of unlike interactions in fluid mixtures, Molecular Simulation 31 (4) (2005) 215–221. doi:10.1080/08927020412331332776.

[77] P. Mausbach, A. Köster, G. Rutkai, M. Thol, J. Vrabec, Comparative study of the Grüneisen parameter for 28 pure fluids, The Journal of Chemical Physics 144 (24) (2016) 244505. doi:10.1063/1.4954282.

[78] D. Bellaire, O. Großmann, K. Münnemann, H. Hasse, Diffusion coefficients at infinite dilution of carbon dioxide and methane in water, ethanol, cyclohexane, toluene, methanol, and acetone: A PFG-NMR and MD simulation study, The Journal of Chemical Thermodynamics 166 (2022) 106691. doi:https://doi.org/10.1016/j.jct.2021.106691.

[79] A. Keller, K. Langenbach, H. Hasse, Comparison of predictions of the PC-SAFT equation of state and molecular sim-

ulations for the metastable region of binary mixtures, Fluid Phase Equilibria 444 (2017) 31–36. `doi:10.1016/j.fluid.2017.04.009`.

[80] M. Kohns, Molecular simulation study of dielectric constants of pure fluids and mixtures, Fluid Phase Equilibria 506 (2020) 112393. `doi:10.1016/j.fluid.2019.112393`.

[81] S. Eckelsbach, M. Bernreuther, C. Engin, G. Guevara-Carrion, Y.-L. Huang, T. Merker, H. Hasse, J. Vrabec, Molecular modeling of hydrogen bonding fluids: Phase behavior of industrial fluids, in: W. E. Nagel, D. B. Kröner, M. M. Resch (Eds.), High Performance Computing in Science and Engineering '11, Springer, Berlin, Heidelberg, 2012, pp. 567–579. `doi:10.1007/978-3-642-23869-7_41`.

[82] S. Werth, M. Horsch, H. Hasse, Molecular simulation of the surface tension of 33 multi-site models for real fluids, Journal of Molecular Liquids 235 (2017) 126–134. `doi:10.1016/j.molliq.2016.12.062`.

[83] G. Guevara-Carrion, T. Janzen, Y. M. Muñoz-Muñoz, J. Vrabec, Molecular simulation study of transport properties for 20 binary liquid mixtures and new force fields for benzene, toluene and CCl4, in: W. E. Nagel, D. H. Kröner, M. M. Resch (Eds.), High Performance Computing in Science and Engineering '16, Springer International Publishing, Cham, 2016, pp. 613–634. `doi:10.1007/978-3-319-47066-5_42`.

[84] S. Eckelsbach, J. Vrabec, Fluid phase interface properties of acetone, oxygen, nitrogen and their binary mixtures by molecular simulation, Physical Chemistry Chemical Physics 17 (40) (2015) 27195–27203. `doi:10.1039/C5CP03415A`.

[85] C. Avendaño, T. Lafitte, A. Galindo, C. S. Adjiman, G. Jackson, E. A. Müller, SAFT-γ force field for the simulation of molecular fluids. 1. A single-site coarse grained model of carbon dioxide, The Journal of Physical Chemistry B 115 (38) (2011) 11154–11169. `doi:10.1021/jp204908d`.

[86] C. Avendaño, T. Lafitte, C. S. Adjiman, A. Galindo, E. A. Müller, G. Jackson, SAFT-γ force field for the simulation of molecular fluids: 2. coarse-grained models of greenhouse gases, refrigerants, and long alkanes, The Journal of Physical Chemistry B 117 (9) (2013) 2717–2733. `doi:10.1021/jp306442b`.

[87] A. Ghoufi, P. Malfreyt, D. J. Tildesley, Computer modelling of the surface tension of the gas–liquid and liquid–liquid interface, Chemical Society Reviews 45 (5) (2016) 1387–1409. `doi:10.1039/C5CS00736D`.

[88] R. A. Zubillaga, A. Labastida, B. Cruz, J. C. Martínez, E. Sánchez, J. Alejandre, Surface tension of organic liquids using the OPLS/AA force field, Journal of Chemical Theory and Computation 9 (3) (2013) 1611–1615. `doi:10.1021/ct300976t`.

[89] K. S. Shing, K. E. Gubbins, K. Lucas, Henry constants in non-ideal fluid mixtures, Molecular Physics 65 (5) (1988) 1235–1252. `doi:10.1080/00268978800101731`.

[90] D. Möller, J. Fischer, Vapour liquid equilibrium of a pure fluid from test particle method in combination with NpT molecular dynamics simulations, Molecular Physics 69 (3) (1990) 463–473. `doi:10.1080/00268979000100341`.

[91] J. Janeček, Long range corrections in inhomogeneous simulations, The Journal of Physical Chemistry B 110 (12) (2006) 6264–6269. `doi:10.1021/jp056344z`.

[92] S. Werth, G. Rutkai, J. Vrabec, M. Horsch, H. Hasse, Long-range correction for multi-site Lennard-Jones models and planar interfaces, Molecular Physics 112 (17) (2014) 2227–2234. `doi:10.1080/00268976.2013.861086`.

[93] J. Walton, D. Tildesley, J. Rowlinson, J. Henderson, The pressure tensor at the planar surface of a liquid, Molecular Physics 48 (6) (1983) 1357–1368. `doi:10.1080/00268978300100971`.

[94] R. Battino (Ed.), Nitrogen and air, 1st Edition, Vol. 10 of Solubility data series, Pergamon Press, New York, 1982.

[95] R. Battino, The Ostwald coefficient of gas solubility, Fluid Phase Equilibria 15 (3) (1984) 231–240. `doi:10.1016/0378-3812(84)87009-0`.

[96] A. Lannung, J. C. Gjaldbæk, S. Rundqvist, E. Varde, G. Westin, The solubility of methane in hydrocarbons, alcohols, water, and other solvents, Acta Chemica Scandinavica 14 (1960) 1124–1128. `doi:10.3891/acta.chem.scand.14-1124`.

[97] M. Yaacobi, A. Ben-Naim, Solvophobic interaction, The Journal of Physical Chemistry 78 (2) (1974) 175–178. `doi:10.1021/j100595a017`.

[98] N. A. Darwish, K. A. M. Gasem, R. L. Robinson, Solubility of methane in cyclohexane and in trans-decalin at temperatures from 323 to 423 K at pressures to 9.6 MPa, Journal of Chemical & Engineering Data 43 (2) (1998) 238–240. `doi:10.1021/je970110u`.

[99] E. S. Hill, W. N. Lacey, Rate of solution of methane in quiescent liquid hydrocarbonsII, Industrial & Engineering Chemistry 26 (12) (1934) 1324–1327. `doi:10.1021/ie50300a026`.

[100] E. Wilhelm, R. Battino, The solubility of gases in liquids. 5. The solubility of N2, O2, CO, and CO2 in cyclohexane at 283 to 313 K, The Journal of Chemical Thermodynamics 5 (1) (1973) 117–120. `doi:10.1016/S0021-9614(73)80068-0`.

[101] T. Merker, N. Franke, R. Gläser, T. Schleid, H. Hasse, Gas Solubility in Binary Liquid Mixtures: Carbon Dioxide in Cyclohexane + Cyclohexanone, Journal of Chemical & Engineering Data 56 (5) (2011) 2477–2481. `doi:10.1021/je101342q`.

[102] G.-I. Kaminishi, C. Yokoyama, T. Shinji, Vapor pressures of binary mixtures of carbon dioxide with benzene, n-hexane and cyclohexane up to 7 MPa, Fluid Phase Equilibria 34 (1) (1987) 83–99. `doi:10.1016/0378-3812(87)85052-5`.

[103] J. H. Dymond, Solubility of a series of gases in cyclohexane and dimethylsulfoxide, The Journal of Physical Chemistry 71 (6) (1967) 1829–1831. `doi:10.1021/j100865a043`.

[104] J. H. Dymond, J. H. Hildebrand, Apparatus for accurate, rapid determinations of solubility of gases in liquids, Industrial & Engineering Chemistry Fundamentals 6 (1) (1967) 130–131. `doi:10.1021/i160021a022`.

[105] L. Patyi, I. Furmer, J. Makranczy, A. Sadilenko, Z. Stepanova, M. Berengarten, Solubilities of gases in certain organic liquids, Journal of Applied Cheimstry of the USSR 51 (6) (1978) 1240–1243.

[106] F. Gironi, R. Lavecchia, A simple method for determining the solubility of gases in liquids: Application to CO_2-cycloparaffin systems, Fluid Phase Equilibria 87 (1) (1993) 153–161. `doi:10.1016/0378-3812(93)85023-F`.

[107] J. C. Gjaldbæk, M. Grahn, H. Fex, B. Högberg, T. Linderot, T. Rosenberg, The solubility of carbon dioxide in perfluoro-n-heptane, normal heptane, cyclo-hexane, carbon tetrachloride, benzene, carbon disulphide and aqueous solution of aerosol, Acta Chemica Scandinavica 7 (1953) 537–544. `doi:10.3891/acta.chem.scand.07-0537`.

[108] P. Luehring, A. Schumpe, Gas solubilities (hydrogen, helium, nitrogen, carbon monoxide, oxygen, argon, carbon dioxide) in organic liquids at 293.2 K, Journal of Chemical & Engineering Data 34 (2) (1989) 250–252. `doi:10.1021/je00056a029`.

[109] R. P. Bell, CLXXXV.—The electrical energy of dipole molecules in solution, and the solubilities of ammonia, hydrogen chloride, and hydrogen sulphide, in various solvents, Journal of the Chemical Society (1931) 1371–1382`doi:10.1039/JR9310001371`.

[110] D. S. Tsiklis, G. M. Svetlova, A study of the solubility of gases in cyclohexane, Zhurnal Fizicheskoi Khimii 32 (7) (1958) 1476–1480.

[111] P. Wiegner, Löslichkeitsmessungen von Chlorwasserstoff in Cyclohexan, Zeitschrift für Elektrochemie und angewandte physikalische Chemie 47 (2) (1941) 163–164. `doi:https://doi.org/10.1002/bbpc.19410470217`.

[112] F. Fairbrother, M. Balkin, CCXV.—Studies in electro-endosmosis. Part V. The electro-endosmosis and surface conductivity against a glass surface of solutions of hydrogen chloride in benzene and other solvents, Journal of the Chemical Society (1931) 1564–1578`doi:10.1039/JR9310001564`.

[113] J. C. Gjaldbaek, J. H. Hildebrand, The solubility of nitrogen in carbon disulfide, benzene, normal- and cyclo-hexane, and in three fluorocarbons, Journal of the American Chemical Society 71 (9) (1949) 3147–3150. `doi:10.1021/ja01177a060`.

[114] J. D. Wild, T. Sridhar, O. E. Potter, Solubility of nitrogen and oxygen in cyclohexane, The Chemical Engineering Journal 15 (2) (1978) 209–214. `doi:10.1016/0300-9467(78)85014-X`.

[115] T. Nitta, T. Akimoto, A. Matsui, T. Katayama, An Apparatus for Precise Measurement of Gas Solubility and Vapor Pressure of Mixed Solvents, Journal of Chemical Engineering of Japan 16 (5) (1983) 352–356. `doi:10.1252/jcej.16.352`.

[116] T. Nitta, Y. Nakamura, H. Ariyasu, T. Katayama, Solubilities of nitrogen in binary solutions of acetone with cyclohexane, benzene, chloroform and 2-propanol, Journal of Chemical Engineering of Japan 13 (2) (1980) 97–103. `doi:10.1252/jcej.`

13.97.

[117] J. Vosmansky, V. Dohnal, Gas solubility measurements with an apparatus of the Ben-Naim—Baer type, Fluid Phase Equilibria 33 (1) (1987) 137–155. `doi:10.1016/0378-3812(87)87008-5`.

[118] W. Klempt, Die Gewinnung von Äthylen aus Koksofengas, Berichte der Gesellschaft für Kohlentechnik 5 (1942) 460–472.

[119] L. R. Field, E. Wilhelm, R. Battino, The solubility of gases in liquids 6. Solubility of N2, O2, CO, CO2, CH4, and CF4 in methylcyclohexane and toluene at 283 to 313 K, The Journal of Chemical Thermodynamics 6 (3) (1974) 237–243. `doi:10.1016/0021-9614(74)90175-X`.

[120] A. S. McDaniel, The absorption of hydrocarbon cases by nonaqueous liquids, The Journal of Physical Chemistry 15 (6) (1911) 587–610. `doi:10.1021/j150123a005`.

[121] S. Srivatsan, W. Gao, K. A. M. Gasem, R. L. Robinson, Solubility of methane in toluene at temperatures from 313 to 423 K at pressures to 8.9 MPa, Journal of Chemical & Engineering Data 43 (4) (1998) 623–625. `doi:10.1021/je9800151`.

[122] M. Elbishlawi, J. R. Spencer, Equilibrium Relations of Two Methane-Aromatic Binary Systems at 150° F., Industrial & Engineering Chemistry 43 (8) (1951) 1811–1815. `doi:10.1021/ie50500a036`.

[123] K. Onda, E. Sada, S. Zinno, Solubilities of methane in various pure hydrocarbon oils, The Journal of the Society of Chemical Industry, Japan 61 (6) (1958) 702–705. `doi:10.1246/nikkashi1898.61.702`.

[124] L. Piskovsky, J. Lakomy, Chemicky Prumysl 15 (12) (1965) 745 – 746.

[125] J. C. Gjaldbæk, E. K. Andersen, W. E. Harvey, N. A. Sörensen, The solubility of carbon dioxide, oxygen, carbon monoxide, and nitrogen in polar solvents, Acta Chemica Scandinavica 8 (1954) 1398–1413. `doi:10.3891/acta.chem.scand.08-1398`.

[126] M. J. Horvath, H. M. Sebastian, K.-C. Chao, Gas chromatograph method for the determination of gas solubility in liquids, Industrial & Engineering Chemistry Fundamentals 20 (4) (1981) 394–396. `doi:10.1021/i100004a017`.

[127] L. Zhang, S. Han, H. Knapp, Solubilities of carbon dioxide in mixtures of n-decane + n-hexadecane and n-heptane + toluene, Chinese Journal of Chemical Engineering 4 (2) (1996) 168–173.

[128] M. S. Belhaj, A. Laurent, N. Midoux, J.-C. Charpentier, Solubility and diffusivity of gases in an organic solution of amine, Chemical Engineering Communications 10 (4-5) (1981) 261–267. `doi:10.1080/00986448108910938`.

[129] S. Yao, H. Chen, Z. Zhu, Study on gas-liquid equilibrium of carbon dioxide-toluene system, Journal of Fuel Chemistry and Technology (4) (1985) 297–304.

[130] G. Just, Löslichkeit von Gasen in organischen Lösungsmitteln, Zeitschrift für Physikalische Chemie 37U (1) (1901) 342–367. `doi:10.1515/zpch-1901-3719`.

[131] E. Shenderei, Y. Zelvenskii, F. Ivanovskii, The solubility of carbon dioxide in methyl ethyl ketone, ethyl acetate, and toluene, under pressure at low temperatures, Khim Prom 5 (1960) 370–374.

[132] C. J. Chang, The solubility of carbon dioxide in organic solvents at elevated pressures, Fluid Phase Equilibria 74 (1992) 235–242. `doi:10.1016/0378-3812(92)85064-F`.

[133] W. Ahmed, W. Gerrard, V. K. Maladkar, Significance of the solubility of hydrogen halides in liquid compounds, Journal of Applied Chemistry 20 (4) (1970) 109–116. `doi:10.1002/jctb.5010200403`.

[134] S. J. O'Brien, E. G. Bobalek, The partial pressure of hydrogen bromide from its solutions in some aprotic solvents at 25°, Journal of the American Chemical Society 62 (11) (1940) 3227–3230. `doi:10.1021/ja01868a094`.

[135] H. C. Brown, J. D. Brady, Solubility of hydrogen chloride at low temperatures. A measure of the basic properties of aromatic nuclei; pi- and sigma-complexes and their role in aromatic substitution, Journal of the American Chemical Society 74 (14) (1952) 3570–3582. `doi:10.1021/ja01134a032`.

[136] A. Jabłoniec, S. Horstmann, J. Gmehling, Experimental determination and calculation of gas solubility data for nitrogen in different solvents, Industrial & Engineering Chemistry Research 46 (13) (2007) 4654–4659. `doi:10.1021/ie061258m`.

[137] M. Levi, Sull'energia basica dell'ossido di nrgento in soluzione, Gazzetta Chimica Italiana 31 (2) (1901) 513–541.

[138] J. Horiuti, On the solubility of gas and coefficient of dilatation by adsorption, Scientific papers of the Institute of Physical

and Chemical Research 17 (1931) 125–256.

[139] P. Tkaczuk, Experimentelle bestimmung der gaslöslichkeit von methan in ketonen und vergleich mit vorausberechneten ergebnissen, University of Dortmund, Germany, Report (1986).

[140] I. G. Podvigailova, B. K. Zeinalov, A. A. Kruglikov, D. T. Radzhabov, E. N. Shagidanov, T. G. Shestakova, Z. V. Korbutova, L. I. Melnikova, Solubility of CO2 in organic solvents, The Soviet Chemical Industry 2 (1970) 19–21.

[141] C. J. Chang, K.-L. Chiu, C.-Y. Day, A new apparatus for the determination of P–x–y diagrams and Henry's constants in high pressure alcohols with critical carbon dioxide, The Journal of Supercritical Fluids 12 (3) (1998) 223–237. `doi: 10.1016/S0896-8446(98)00076-X`.

[142] S. Zeck, Beitrag zur experimentellen Untersuchung und Berechnung von Gas-Flüssigkeits-Phasengleichgewichten, Ph.D. thesis, Technische Universität Berlin (1985).

[143] M. Jödecke, A. Pérez-Salado Kamps, G. Maurer, Experimental investigation of the solubility of CO2 in (acetone + water), Journal of Chemical & Engineering Data 52 (3) (2007) 1003–1009. `doi:10.1021/je600571v`.

[144] E. Bodor, B. Mohai, G. Pfeifer, Gas-absorption studies. VII. Absorption of acetylene and carbon dioxide in acetaldehyde, Veszpremi Vegyipari Egyetem Kozlemenyei 3 (1959) 205–210.

[145] O. Stern, Zur kinetischen Theorie des osmotischen Drucks konzentrierter Lösungen und über die Gültigkeit des Henry sehen Gesetzes für konzentrierte Lösungen von Kohlendioxyd in organischen Lösungsmitteln bei tiefen Temperaturen, Zeitschrift für Physikalische Chemie 81U (1) (1913) 441–476. `doi:10.1515/zpch-1913-8124`.

[146] W. A. Felsing, S. A. Durban, The vapor pressures, densities, and some derived quantities for acetone, Journal of the American Chemical Society 48 (11) (1926) 2885–2893. `doi:10.1021/ja01690a020`.

[147] H. Hsu, D. Campbell, Formulations with soluble gas propellants, Aerosol Age 9 (1964) 34.

[148] E. Otsuka, M. Takada, Studies on purification of acetylene from the burner gas formed by partial oxidation of methane (I), Journal of the Fuel Society of Japan 42 (4) (1963) 229–237. `doi:10.3775/jie.42.229`.

[149] F. W. Giacobbe, Thermodynamic solubility behavior of carbon dioxide in acetone, Fluid Phase Equilibria 72 (1992) 277–298. `doi:10.1016/0378-3812(92)85031-3`.

[150] C. Liu, C.-x. Li, H. Meng, Z.-h. Wang, Solubility of trifluoromethane and hydrochloride gas in different solvents, Journal of Chemical Engineering of Chinese Universities 22 (1) (2008) 1–5.

[151] T. Windmann, A. Köster, J. Vrabec, Vapor–Liquid Equilibrium Measurements of the Binary Mixtures Nitrogen + Acetone and Oxygen + Acetone, Journal of Chemical & Engineering Data 57 (6) (2012) 1672–1677. `doi:10.1021/je201058j`.

[152] C. B. Kretschmer, J. Nowakowska, R. Wiebe, Solubility of oxygen and nitrogen in organic solvents from -25° to 50° C, Industrial & Engineering Chemistry 38 (5) (1946) 506–509. `doi:10.1021/ie50437a018`.

[153] K. Tsuji, K. Ichikawa, H. Yamamoto, J. Tokunaga, Solubilities of oxygen and nitrogen in acetone-water mixed solvent, Kagaku Kogaku Ronbunshu 13 (6) (1987) 825–830. `doi:10.1252/kakoronbunshu.13.825`.

[154] T. Tominaga, R. Battino, H. K. Gorowara, R. D. Dixon, E. Wilhelm, Solubility of gases in liquids. 17. The solubility of helium, neon, argon, krypton, hydrogen, nitrogen, oxygen, carbon monoxide, methane, carbon tetrafluoride, and sulfur hexafluoride in tetrachloromethane at 283 to 318 K, Journal of Chemical & Engineering Data 31 (2) (1986) 175–180. `doi:10.1021/je00044a014`.

[155] P. Maltese, F. Alborno, Equilibrio liquido-vapore del sistema acido cloridrico-1,2-dicloroetano, La Chimica e L'Industria 46 (1964) 1317–1321.

[156] J. J. Howland, D. R. Miller, J. E. Willard, The solubilities of hydrogen chloride and hydrogen bromide in carbon tetrachloride and in chloroform, Journal of the American Chemical Society 63 (10) (1941) 2807–2811. `doi:10.1021/ja01855a090`.

[157] M. Curda, J. Holas, The solubility of chlorine, hydrogen chloride and methyl chloride in some solvents, Chemicky Prumysl 14 (10) (1964) 547–548.

[158] T. Akimoto, T. Nitta, T. Katayama, Nitrogen solubility and vapor pressure of binary mixed solvents containing benzene, carbon tetrachloride, cyclohexane and 1-hexane., Journal of Chemical Engineering of Japan 17 (6) (1984) 637–641. doi:10.1252/jcej.17.637.

[159] J. K. Wolfe, Discussion - "Solubility of air in Freon-12 and Freon-22", Refrigerating Engineering 59 (1951) 669–706.

[160] M. Konieczny, G. Sosnovsky, Novel aspects in the preparation of phorone, Zeitschrift für Naturforschung B 33 (4) (1978) 454–460. doi:10.1515/znb-1978-0421.

[161] N. Hayer, F. Jirasek, H. Hasse, Prediction of Henry's law constants by matrix completion, AIChE Journal 68 (9) (2022) e17753. doi:10.1002/aic.17753.

[162] W. Hayduk, W. D. Buckley, Temperature coefficient of gas solubility for regular solutions, The Canadian Journal of Chemical Engineering 49 (5) (1971) 667–671. doi:10.1002/cjce.5450490520.

[163] X. Tang, J. Gross, Renormalization-group corrections to the perturbed-chain statistical associating fluid theory for binary mixtures, Industrial & Engineering Chemistry Research 49 (19) (2010) 9436–9444. doi:10.1021/ie100890d.

[164] E. Kiran, P. G. Debenedetti, C. J. Peters (Eds.), Supercritical Fluids - Fundamentals and Applications, Vol. 273 of NATO Science Series, Kluwer Academic Publishers, Kemer, Antalya, Turkey, 1998.

[165] M. Y. Belyakov, E. E. Gorodetskii, Universal crossover approach to equation of state for fluids, International Journal of Thermophysics 27 (5) (2006) 1387–1405. doi:10.1007/s10765-006-0101-y.

[166] S. Stephan, J. Liu, K. Langenbach, W. G. Chapman, H. Hasse, Vapor-liquid interface of the lennard-jones truncated and shifted fluid: Comparison of molecular simulation, density gradient theory, and density functional theory, The Journal of Physical Chemistry C 122 (43) (2018) 24705–24715. doi:10.1021/acs.jpcc.8b06332.

[167] S. Stephan, K. Langenbach, H. Hasse, Enrichment of components at vapour - liquid interfaces: A study by molecular simulation and density gradient theory, Chemical Engineering Transactions 69 (2018) 295–300. doi:10.3303/CET1869050.

[168] A. Mejía, M. Cartes, H. Segura, E. A. Müller, Use of equations of state and coarse grained simulations to complement experiments: Describing the interfacial properties of carbon dioxide + decane and carbon dioxide + eicosane mixtures, Journal of Chemical & Engineering Data 59 (10) (2014) 2928–2941. doi:10.1021/je5000764.

[169] J. M. Garrido, M. Cartes, A. Mejía, Coarse-grained theoretical modeling and molecular simulations of nitrogen + n-alkanes: (n-pentane, n-hexane, n-heptane, n-octane), The Journal of Supercritical Fluids 129 (2017) 83–90. doi:10.1016/j.supflu.2017.01.001.

[170] I. Nitzke, R. Stierle, S. Stephan, M. Pfitzner, J. Gross, J. Vrabec, Phase equilibria and interface properties of hydrocarbon propellant–oxygen mixtures in the transcritical regime, Physics of Fluids 35 (3) (2023) 032117. doi:10.1063/5.0138973.

[171] B. González-Barramuño, E. Cea-Klapp, I. Polishuk, R. I. Canales, H. Quinteros-Lama, J. M. Garrido, Interfacial properties of fluorinated (F)-gases in azeotropic condition, Journal of Molecular Liquids 350 (2022) 118604. doi:10.1016/j.molliq.2022.118604.

[172] A. Mejía, M. Cartes, H. Segura, Interfacial tensions of binary mixtures of ethanol with octane, decane, dodecane, and tetradecane, The Journal of Chemical Thermodynamics 43 (9) (2011) 1395–1400. doi:10.1016/j.jct.2011.04.005.

[173] W. A. Fouad, L. F. Vega, The phase and interfacial properties of azeotropic refrigerants: the prediction of aneotropes from molecular theory, Physical Chemistry Chemical Physics 19 (13) (2017) 8977–8988. doi:10.1039/C6CP08031F.

[174] S. Werth, K. Stöbener, P. Klein, K.-H. Küfer, M. Horsch, H. Hasse, Molecular modelling and simulation of the surface tension of real quadrupolar fluids, Chemical Engineering Science 121 (2015) 110–117. doi:10.1016/j.ces.2014.08.035.

[175] S. Werth, M. Horsch, H. Hasse, Molecular simulation of the surface tension of 33 multi-site models for real fluids, Journal of Molecular Liquids 235 (2017) 126–134. doi:10.1016/j.molliq.2016.12.062.

[176] S. Werth, Molecular modeling and simulation of vapor-liquid interfaces, Ph.D. thesis, Technische Universität Kaiserslautern (2016).

[177] S. Stephan, S. Becker, K. Langenbach, H. Hasse, Vapor-liquid interfacial properties of the system cyclohexane + CO2:

Experiments, molecular simulation and density gradient theory, Fluid Phase Equilibria 518 (2020) 112583. `doi:10.1016/j.fluid.2020.112583`.

[178] S. Senapati, M. L. Berkowitz, Computer simulation study of the interface width of the liquid/liquid interface, Physical Review Letters 87 (17) (2001) 176101. `doi:10.1103/PhysRevLett.87.176101`.

[179] P. Tarazona, E. Chacón, F. Bresme, Intrinsic profiles and the structure of liquid surfaces, Journal of Physics: Condensed Matter 24 (28) (2012) 284123. `doi:10.1088/0953-8984/24/28/284123`.